

# Experimental and Computational Studies of Hydrogen Bonding and Proton Transfer to [Cp\*Fe(dppe)H]

Natalia V. Belkova,<sup>[a]</sup> Edmond Collange,<sup>[b]</sup> Pavel Dub,<sup>[a]</sup> Lina M. Epstein,<sup>[a]</sup> Dmitrii A. Lemenovskii,<sup>[c]</sup> Agustí Lledós,<sup>\*,[d]</sup> Olivier Maresca,<sup>[d]</sup> Feliu Maseras,<sup>[d]</sup> Rinaldo Poli,<sup>\*,[e]</sup> Pavel O. Revin,<sup>[a, c]</sup> Elena S. Shubina,<sup>\*,[a]</sup> and Evgenii V. Vorontsov<sup>[a]</sup>

**Abstract:** The present contribution reports experimental and computational investigations of the interaction between [Cp\*Fe(dppe)H] and different proton donors (HA). The focus is on the structure of the proton transfer intermediates and on the potential energy surface of the proton transfer leading to the dihydrogen complex [Cp\*Fe(dppe)(H<sub>2</sub>)]<sup>+</sup>. With *p*-nitrophenol (PNP) a UV/Visible study provides evidence of the formation of the ion-pair stabilized by a hydrogen bond between the nonclassical cation [Cp\*Fe(dppe)(H<sub>2</sub>)]<sup>+</sup> and the homoconjugated anion ([AHA]<sup>−</sup>). With trifluoroacetic acid (TFA), the hydrogen-bonded ion pair containing the simple

conjugate base (A<sup>−</sup>) in equilibrium with the free ions is observed by IR spectroscopy when using a deficit of the proton donor. An excess leads to the formation of the homoconjugated anion. The interaction with hexafluoroisopropanol (HFIP) was investigated quantitatively by IR spectroscopy and by <sup>1</sup>H and <sup>31</sup>P NMR spectroscopy at low temperatures (200–260 K) and by stopped-flow kinetics at about room temperature (288–308 K). The hydro-

**Keywords:** density functional calculations • dihydrogen bonding • hydride ligands • iron • proton transfer

gen bond formation to give [Cp\*Fe(dppe)H]⋯HA is characterized by  $\Delta H^\circ = -6.5 \pm 0.4 \text{ kcal mol}^{-1}$  and  $\Delta S^\circ = -18.6 \pm 1.7 \text{ cal mol}^{-1} \text{ K}^{-1}$ . The activation barrier for the proton transfer step, which occurs only upon intervention of a second HFIP molecule, is  $\Delta H^\ddagger = 2.6 \pm 0.3 \text{ kcal mol}^{-1}$  and  $\Delta S^\ddagger = -44.5 \pm 1.1 \text{ cal mol}^{-1} \text{ K}^{-1}$ . The computational investigation (at the DFT/B3LYP level with inclusion of solvent effects by the polarizable continuum model) reproduces all the qualitative findings, provided the correct number of proton donor molecules are used in the model. The proton transfer process is, however, computed to be less exothermic than observed in the experiment.

## Introduction

Proton transfer processes to and from transition-metal centers and hydride ligand sites are of fundamental importance for catalysis and are also relevant to the biochemical genesis of dihydrogen.<sup>[1]</sup> It has now been quite firmly established

that when both a hydride ligand and a metal-based electron pair are present in the same complex, proton donors show a kinetic preference for the hydride site,<sup>[2–8]</sup> though exceptions have recently been reported from studies carried out in our laboratories.<sup>[9,10]</sup> It has also been established that hydrogen-bonded adducts are well-defined intermediates along the


[a] Dr. N. V. Belkova, P. Dub, Prof. L. M. Epstein, P. O. Revin, D.Sc. E. S. Shubina, Dr. E. V. Vorontsov  
Nesmeyanov Institute of Organoelement Compounds (INEOS) Russian Academy of Sciences, Vavilov Street 28, 119991 Moscow (Russia)  
E-mail: shu@ineos.ac.ru

[b] Dr. E. Collange  
Laboratoire de Synthèse et d'Electrosynthèse Organométalliques (LSEO UMR 5632)  
Université de Bourgogne, Faculté de Sciences "Gabriel", 6 boulevard Gabriel, 21000 Dijon (France)

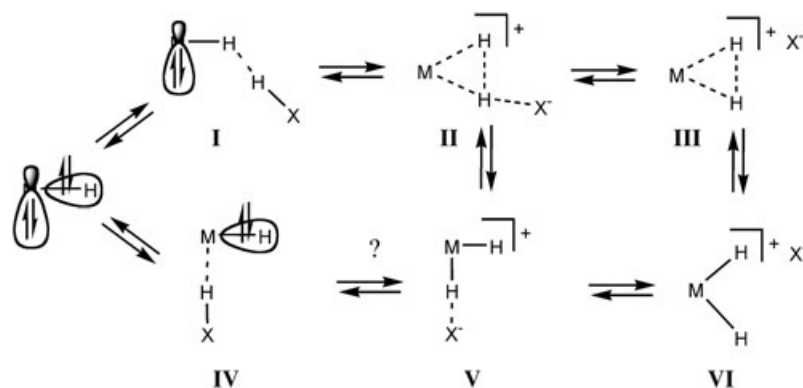
[c] Prof. D. A. Lemenovskii, P. O. Revin  
Chemistry Department  
Moscow State University, Vorob'evy Gory, 119899 Moscow (Russia)

[d] Prof. A. Lledós, Dr. O. Maresca, Prof. F. Maseras  
Departament de Química  
Edifici Cn, Universitat Autònoma de Barcelona  
08193 Bellaterra (Spain)  
E-mail: agusti@klngon.uab.es

[e] Prof. R. Poli  
Laboratoire de Chimie de Coordination (LCC UPR 8241)  
205 Route de Narbonne, 31077 Toulouse Cedex (France)  
Fax: (+33) 561-553-003  
E-mail: poli@lcc-toulouse.fr

 Supporting information for this article is available on the WWW under <http://www.chemeurj.org/> or from the author.

proton transfer pathway.<sup>[11–13]</sup> Thus, referring to the general Scheme 1, species **II** or **III** are usually generated faster than species **V** or **VI**, a phenomenon that is not necessarily related to the thermodynamic preference for hydrogen bond formation at the hydride (**I**) or metal (**IV**) site. Whether indeed there is a general correlation between the strength of the hydrogen bonding at a particular site and the rate of proton transfer at the same site is not yet known.



Scheme 1.

The kinetics of proton transfer to the hydride ligand has been studied for several iron subgroup complexes. A number of different acids (HBF<sub>4</sub>, CF<sub>3</sub>CO<sub>2</sub>H, CF<sub>3</sub>SO<sub>3</sub>H, HCl, HBr) were used by Basallote et al.,<sup>[14–18]</sup> but they were too strong to identify hydrogen-bonded intermediates, and species like **I** or **II** have been only anticipated as transition states. More recent work, on the other hand, has provided kinetic evidence for the importance of species **II** in the reverse deprotonation reaction for the complex *trans*-[FeH(η<sup>2</sup>-H<sub>2</sub>)(dppe)<sub>2</sub>]<sup>+</sup>.<sup>[19]</sup> Some of us have studied the kinetics of the transformation of the dihydrogen-bonded complex **I** into the nonclassical complex **II** in the case of [CpRuH(CO)(PCy<sub>3</sub>)] by using fluorinated alcohols as proton donors.<sup>[20]</sup> The activation enthalpy and entropy of the proton transfer process as well as the thermodynamic parameters for the dihydrogen bond formation step have been obtained for the protonation by perfluoro-*tert*-butanol (PFTB) in hexane. The low solubility of the ion-paired complex in hexane prevented us from determining the equilibrium thermodynamic parameters of the proton transfer step. The enthalpies and entropies of both the dihydrogen bond and the molecular hydrogen complex formation steps have been obtained for [(triphos)-Re(CO)<sub>2</sub>H]/PFTB,<sup>[21]</sup> [(triphos)Ru(CO)H<sub>2</sub>]/HFIP,<sup>[22]</sup> [PP<sub>3</sub>OsH<sub>2</sub>]/TFE,<sup>[23]</sup> and [RuH<sub>2</sub>(dppm)<sub>2</sub>]/HFIP<sup>[24]</sup> systems (triphos = CH<sub>3</sub>C(CH<sub>2</sub>PPh<sub>2</sub>)<sub>3</sub>; PP<sub>3</sub> = P(CH<sub>2</sub>CH<sub>2</sub>PPh<sub>2</sub>)<sub>3</sub>; dppm = Ph<sub>2</sub>PCH<sub>2</sub>PPh<sub>2</sub>; HFIP = hexafluoroisopropanol, TFE = 2,2,2-trifluoroethanol). The protonation of these hydrides is exothermic and exoentropic, the equilibrium shifting toward cationic dihydrogen complexes upon cooling. However, the proton transfer step was too fast to be studied by conventional spectroscopic methods (IR, NMR) and no activation

data were derived. To date, there is no example in the literature where both activation and equilibrium thermodynamic data have been determined for the same system and where a quantitative energy profile can be presented for the proton transfer process to a transition-metal hydride.

Some of us have recently reported an experimental study of the protonation of the complex [Cp\*FeH(dppe)] in CH<sub>2</sub>Cl<sub>2</sub> with a variety of proton donors of different acid strength (2-monofluoroethanol, MFE; TFE; HFIP; PFTB; and trifluoroacetic acid, TFA).<sup>[25]</sup> Using weaker acids, we have not only confirmed the results of Hamon et al.<sup>[5,6]</sup> for the protonation with HBF<sub>4</sub> whereby the proton transfer is faster at the hydride site to give an intermediate dihydrogen complex, [Cp\*Fe(H<sub>2</sub>)(dppe)]<sup>+</sup>, but also found the spectroscopic signatures for the establishment of a hydrogen bond at the hydride site. Furthermore, we have determined the thermodynamic characteristics of this interaction. No evidence was obtained

for the establishment of a hydrogen bond with the metal center. We have also determined experimentally that the fluorinated alcohols are able to transfer the proton only with assistance from a second alcohol molecule. No information of this kind could be obtained in the case of trifluoroacetic acid (TFA), because of the faster rate of the proton transfer process. In addition, we have established that the isomerization yielding the final classical dihydride product [Cp\*FeH<sub>2</sub>(dppe)]<sup>+</sup> occurs by means of an internal rearrangement process rather than a reversible deprotonation at the hydride site followed by a slower protonation at the metal site.<sup>[25]</sup> This conclusion followed the key observation that the rate of isomerization is independent of the nature of the proton donor, whereas the rate of proton transfer at the hydride site increases with the hydrogen bond strength.

The main aim of the present study is to obtain more detailed information on the structure of the proton transfer intermediates and on the proton transfer potential energy surface, specifically: 1) the role of the second proton donor molecule; 2) the hydrogen bonding status in the intermediate dihydrogen complex (i.e. as **II** or **III**) and final product (i.e. as **V** or **VI**); 3) the energetic cost of the proton transfer process and of the subsequent internal rearrangement leading to the final dihydride product; 4) the intimate mechanism of this rearrangement. To address these questions, we have carried out new experimental studies with additional proton donors that contain UV/Vis and IR spectroscopic probes that are more sensitive to the chemical environment for the deprotonated acid. We have undertaken careful equilibrium investigations of the proton transfer step for the [Cp\*Fe(dppe)H]/HFIP system. We have carried out a varia-

ble-temperature stopped-flow kinetic study of the same proton transfer process to gain information on the activation parameters for the proton transfer step. Finally, we have completed our study with a computational investigation of the energetics of hydrogen bonding at the hydride and metal sites, as well as the potential energy surface for the proton transfer process at both sites. Herein, we present the new spectroscopic results, the variable-temperature stopped-flow results, and the computational analysis of the proton transfer step and on the intimate nature of the conjugate base. An accompanying computational study of the rearrangement mechanism will be presented separately.<sup>[26]</sup>

## Experimental Section

All manipulations were carried out under an argon atmosphere by standard Schlenk techniques. The [Cp\*Fe(dppe)H] hydride was synthesized according to reference [27].

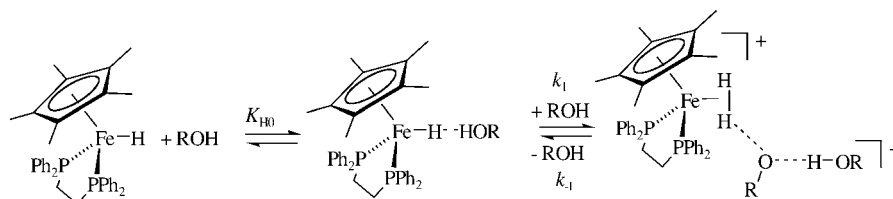
**IR and UV/Vis investigations:** IR measurements were performed with a "Specord M82" spectrometer (IR) on 0.1–0.15 M (for the  $\nu(\text{OH})$  measurements) or 0.02–0.025 M (for the  $\nu(\text{MH})$ ,  $\nu(\text{CO})$  and  $\nu^{\text{as}}(\text{OCO})$  measurements) hydride solutions in  $\text{CH}_2\text{Cl}_2$  (0.12 cm path length) using  $\text{CaF}_2$  cells. UV measurements were performed on Specord M-40 and Varian Cary 5 spectrophotometers in  $\text{CH}_2\text{Cl}_2$ . Low-temperature IR and UV measurements were carried out by using a cryostat (Carl Zeiss Jena) in the 200–290 K temperature range. The accuracy of the temperature adjustment was  $\pm 0.5$  K. The reagents were mixed at low temperature and the cold mixtures were subsequently transferred into the pre-cooled cryostat.

Variable-temperature UV/Vis spectra of the homoconjugated PNP anion were obtained for the equimolar mixture of PNP and potassium *p*-nitrophenolate in the presence of excess [18]crown-6. As was shown by independent measurements, PNP forms a hydrogen-bonded adduct with the crown ether with a band at 330–346 nm. Subtraction of this band from the spectra gives the band of the homoconjugated PNP anion presented in Figure 1.

**NMR investigations:** NMR studies were carried out in standard 5-mm NMR tubes containing solutions of the complexes in  $\text{CD}_2\text{Cl}_2$ . The  $^1\text{H}$  and  $^{31}\text{P}$  NMR data were collected with a Bruker AMX 400 spectrometer operating at 400.13 and 161.98 MHz, respectively. The spectra were calibrated

with the residual protonated solvent resonance ( $^1\text{H}$ ) and with external 85%  $\text{H}_3\text{PO}_4$  ( $^{31}\text{P}$ ). The conventional inversion-recovery method (180– $\tau$ –90) was used to determine the variable-temperature longitudinal relaxation time  $T_1$ . Low temperature experiments were carried out in the 180–260 K temperature range by using a TV-3000 Bruker temperature unit. The apparatus was calibrated with a methanol standard. The accuracy and stability of temperature was  $\pm 1$  K. All samples were allowed to equilibrate at every temperature for at least 10 min. All mixings between the alcohols and the hydride complexes were performed at low temperature.

**Proton transfer equilibrium constants from NMR and UV/Vis data:** For the calculation of the proton transfer equilibrium constant leading from [Cp\*Fe(dppe)H]...HOR and ROH to [Cp\*Fe(dppe)(H<sub>2</sub>)]<sup>+</sup>...[ROHOR]<sup>−</sup> [ $\text{R} = (\text{CF}_3)_2\text{CH}$ ] ( $K_1 = k_1/k_{-1}$ , see Scheme 2), the concentration of



Scheme 2.

[Cp\*Fe(dppe)(H<sub>2</sub>)]<sup>+</sup>...[ROHOR]<sup>−</sup>, on one side, and the sum of [Cp\*Fe(dppe)H] and [Cp\*Fe(dppe)H]...HOR, on the other side, were derived from the measured relative intensities of the significant NMR resonances (hydride ligand resonance in the  $^1\text{H}$  NMR spectrum and phosphine resonance in the  $^{31}\text{P}$  NMR spectrum) or from the measured intensity of the UV band in comparison with the spectra of pure [Cp\*Fe(dppe)H] and [Cp\*Fe(dppe)(H<sub>2</sub>)]<sup>+</sup>. The UV/Vis spectrum of pure [Cp\*Fe(dppe)H] did not change upon formation of the hydrogen bonded adduct [Cp\*Fe(dppe)H]...HOR as verified by the stopped-flow experiment. The spectrum of pure [Cp\*Fe(dppe)(H<sub>2</sub>)]<sup>+</sup> was obtained by low-temperature (200 K) protonation with  $\text{HBF}_4$  and it is also assumed to be independent from the hydrogen bonding with the [ROHOR]<sup>−</sup> homoconjugated anion.

The sum of [Cp\*Fe(dppe)H] and [Cp\*Fe(dppe)H]...HOR equilibrium concentrations could be partitioned to the individual species, given the independent knowledge of  $K_{\text{H0}}$  (see Results section) and the calculation of [ROH] from Equation (1). Using  $K_{\text{H0}}$  to express [[Cp\*Fe(dppe)H]...HOR] as a function of [ROH] and ([Cp\*Fe(dppe)H] + [[Cp\*Fe(dppe)H]...HOR]) and insertion into Equation (1) gives a quadratic equation from which the concentration [ROH] can be calculated. From that, the calculation of  $K_1$  is straightforward.

$$[\text{ROH}] = C_{\text{ROH}} - [[\text{Cp}^*\text{Fe}(\text{dppe})\text{H}] \cdots \text{HOR}] - 2[[\text{Cp}^*\text{Fe}(\text{dppe})(\text{H}_2)]^+ \cdots [\text{ROHOR}]^-] \quad (1)$$

**Stopped-flow investigations:** The stopped-flow kinetic runs were carried out in the temperature range 15–35 °C with a Hitech SF-61-DX2 apparatus coupled to a Hitech diode-array UV/Visible spectrophotometer. Given the extreme air-sensitivity of the hydride compound, unacceptable results were obtained at the low concentrations required for work in a suitable absorbance range when using a regular 1 cm cell (ca.  $5 \times 10^{-4}$  M). This phenomenon is attributed to oxidation by oxygen diffusion through the instrument transfer lines, as confirmed by the observation of small and irreproducible signal evolutions when shooting the same hydride solution from both syringes. Switching to a tenfold concentration and to a smaller path length (1.5 mm) reduced the oxidation problem below acceptable noise levels. Only the data that were collected within the first 2 s were analyzed, and these yielded reproducible results. The temperature range was limited by the fact that the instrument leaks at  $T < 15$  °C,

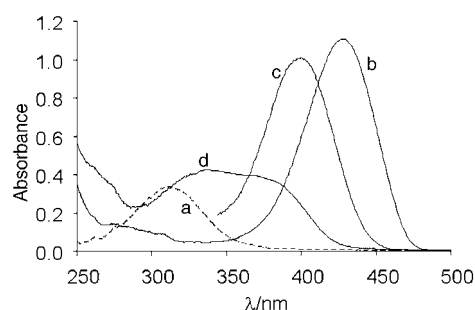


Figure 1. UV/Vis spectra at 200 K in  $\text{CH}_2\text{Cl}_2$  of a) PNP (0.001 M); b) potassium *p*-nitrophenolate (0.001 M in the presence of [18]crown-6); c) homoconjugated PNP anion (band derived from the spectrum of a 1:1 mixture of (a) and (b)); d) PNP (0.001 M) in the presence of [Cp\*FeH(dppe)] (0.0005 M).

whereas it is too tight at  $T > 35^\circ\text{C}$ . All experiments were run with the same stock solutions during the same day. After each temperature change, the thermal equilibrium was reached within approximately 15 min and was checked by the reproducibility of the first few shots. At least three shots were used at each temperature to obtain the averaged results reported in the Results section. The rate data were obtained by a global fit using the SPECFIT software.<sup>[28]</sup>

**Computational details:** Quantum computations were performed with the Gaussian98<sup>[29]</sup> package at the DFT/B3LYP level.<sup>[30–32]</sup> Core electrons of the Fe and of the P atoms were described by using the effective core pseudopotentials of Hay–Wadt<sup>[33,34]</sup> and valence electrons were described with a standard double- $\zeta$  basis set.<sup>[29]</sup> In the case of the P atoms, a set of d-type functions was added to the standard basis functions.<sup>[35]</sup> Carbon atoms and hydrogen atoms nonbonded to the metal together with atoms of proton donors (C, F, H) not involved in hydrogen bonds were described with a 6–31G basis set.<sup>[36]</sup> The hydrogen atom directly bonded to the Fe atom together with hydrogen and oxygen atoms of the proton donors involved in hydrogen bonding were then described with a 6–31G(d,p) set of basis functions.<sup>[37]</sup> Solvent effects were taken into account by means of polarized continuum model (PCM) calculations<sup>[38,39]</sup> using standard options.<sup>[29]</sup> The free energies of solvation were then computed in dichloromethane ( $\epsilon = 8.93$ ) at the geometries optimized in the gas phase. The complexation energies in the gas phase were also corrected from the basis set superposition errors according to the counterpoise method of Boys and Bernardi.<sup>[40]</sup> Test calculations on the real complex  $[\text{Cp}^*\text{Fe}(\text{dppe})\text{H}]$  were carried out using the IMOMM method,<sup>[41]</sup> with a program built from modified versions of Gaussian98<sup>[29]</sup> for the quantum mechanics part and mm3(92)<sup>[42]</sup> for the molecular mechanics part. The  $[\text{Cp}^*\text{Fe}(\text{dppe})\text{H}]$  ( $\text{dppe} = \text{PH}_2\text{CH}_2\text{CH}_2\text{PH}_2$ ) plus the proton donor constituted the quantum mechanical part (QM) of the system while the four phenyl ligands were described by molecular mechanics (MM). The QM part of the calculations was done at the B3LYP level using the same basis defined previously. The MM part calculations used the mm3(92) force field.<sup>[43]</sup> Torsional contributions involving dihedral angles with the metal center were set to zero. All of the geometrical parameters were optimized except the bond lengths of atoms involved in the QM-MM frontier. The frozen values were 1.41 Å for the P–H bonds of the  $[\text{Cp}^*\text{Fe}(\text{dppe})]$  in the quantum part and the crystallographic values for the P–C in the MM part.

## Results

### Interaction of $[\text{Cp}^*\text{FeH}(\text{dppe})]$ with PNP: UV/Vis study:

The absorptions of substituted phenols in the visible spectrum are highly characteristic of their protonation and hydrogen bonding state.<sup>[44–46]</sup> Therefore, we used *p*-nitrophenol (PNP) to distinguish between all species in equilibrium. Whereas the visible bands of the phenol ( $\text{ArOH}$ ), of its conjugate base ( $[\text{ArO}]^-$ ), and of the homoconjugated anion ( $[\text{ArOHOAr}]^-$ ) are centered at different positions as shown in Table 1, the bands of the hydrogen-bonded complexes  $\text{ArOH}\cdots[\text{X}]^-$  and  $[\text{ArO}]^-\cdots\text{HX}$ , appear at intermediate positions.<sup>[47]</sup> The exact band positions are dependent on the solvent<sup>[46]</sup> and temperature. The values obtained in this work

Table 1. Visible bands ( $\lambda_{\text{max}}$  [nm]) and their molar absorption coefficients ( $\epsilon$  [ $\text{L mol}^{-1}\text{cm}^{-1}$ ]) of the free *p*-nitrophenol and its conjugate base in  $\text{CH}_2\text{Cl}_2$ .

$T$ [K]	ArOH	$[\text{ArOHOAr}]^-$	$[\text{ArO}]^-$
280	305 (8050)	398 (19750)	423 (21250)
200	312 (9970)	400 (25250)	430 (27605)

for  $\text{CH}_2\text{Cl}_2$  solutions (Table 1) are in good agreement with the literature data. Figure 1 shows the spectra of the key species obtained.

Visible spectra were recorded for  $\text{CH}_2\text{Cl}_2$  solutions of PNP (0.001–0.003 M) in the presence of  $[\text{Cp}^*\text{FeH}(\text{dppe})]$  at different concentrations (PNP/Fe ratios from 1:0.1 to 1:2) and at temperatures between 200 K and room temperature. The spectra show wide bands with a complex shape, resulting from the overlap of both the phenol in its various forms and the iron hydride complexes (both free and dihydrogen bonded). The latter bands are wide (for  $[\text{Cp}^*\text{FeH}(\text{dppe})]$  the half-height band width  $\Delta\lambda_{1/2}$  is ca. 130 nm)<sup>[48]</sup> and have lower molar absorption coefficients (for  $[\text{Cp}^*\text{FeH}(\text{dppe})]$   $\epsilon$  ( $\lambda_{\text{max}} = 388\text{ nm}$ ) =  $2370\text{ L mol}^{-1}\text{cm}^{-1}$  at 200 K). Therefore, they contribute only in a minor way to the total absorption, affecting mainly quantitative results. An analysis of the spectral changes indicates the overlap of three bands, with maxima centered respectively at 312, 340, and 380 nm. On the basis of literature precedents, the following assignments could be made: on the acid side, the band centered at 312 nm is assigned to free PNP and the band at 340 nm is assigned to the nonclassical dihydrogen bonded complex  $[\text{Cp}^*(\text{dppe})\text{FeH}]\cdots\text{HOAr}$  ( $\text{Ar} = p\text{-C}_6\text{H}_4\text{NO}_2$ ). The 28 nm red shift is caused by the effect of hydrogen bonding on the electronic absorption by the phenol chromophore. On the conjugate base side, the band at 380 nm is attributed to a hydrogen-bonded phenolate ion, since this is blue-shifted from the free phenolate band by approximately 50 nm. The absence of free phenolate is signaled by the absence of a band at 430 nm. There are two possibilities for this species: the hydrogen-bonded ion pair  $[\text{Cp}^*(\text{dppe})\text{Fe}(\text{H}_2)]^+\cdots[\text{OAr}]^-$ , and the homoconjugated anion  $[\text{ArOHOAr}]^-$ . The latter could either be free or further hydrogen bonded to the cationic dihydrogen complex.

Upon increasing the amount of  $[\text{Cp}^*\text{Fe}(\text{dppe})\text{H}]$  at constant initial phenol concentration and at constant temperature, the bands at 340 nm and 380 nm grew in intensity, whereas the free phenol band at 312 nm decreased (Figure 2). The plot of the intensity changes at 380 nm versus the  $[\text{Cp}^*(\text{dppe})\text{FeH}]$  mole fraction [Eq. (2)] gives a break point for a mole fraction of (or near) 0.3, indicating a 1:2 binding stoichiometry for the ionic species,  $[\text{Cp}^*(\text{dppe})\text{Fe}(\text{H}_2)]^+[\text{ArOHOAr}]^-$ , see Figure 3.<sup>[49]</sup> The blue-shift of

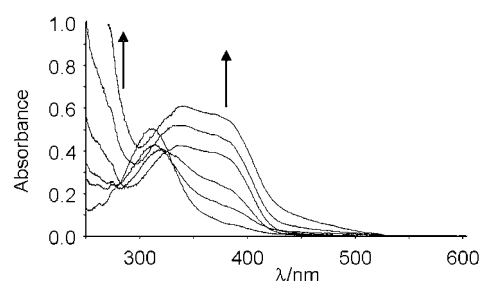


Figure 2. UV/Vis spectra for a  $\text{CH}_2\text{Cl}_2$  solution containing PNP (0.001 M) and  $[\text{Cp}^*\text{FeH}(\text{dppe})]$  at 200 K. The Fe/PNP molar ratios are, respectively (bottom to top): 0.1, 0.2, 0.3, 0.5, 1, and 2.

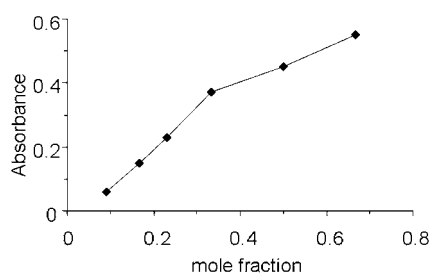


Figure 3. Intensity changes at 380 nm versus the [Cp\*(dppe)FeH] mole fraction. The data are from the UV/Vis spectra shown in Figure 2.

this band relative to free [ArOHOAr]<sup>−</sup> (Table 1), suggests further hydrogen bonding of homoconjugated anion with the cationic dihydrogen complex, [Cp\*(dppe)Fe(H<sub>2</sub>)]<sup>+</sup>...[ArOHOAr]<sup>−</sup>.

$$\text{mole fraction} = C_{\text{FeH}} / [C_{\text{FeH}} + C_{\text{PNP}}] \quad (2)$$

The spectral changes are fully reversible in the 200–260 K temperature range, showing that no significant isomerization to the classical dihydride complex occurs below 260 K in agreement with our previous report.<sup>[25]</sup> Upon lowering the temperature, the band of the free phenol decreases and those of hydrogen-bonded phenol (340 nm) and hydrogen-bonded ion pair (380 nm) increase (Figure 4). Note that nei-

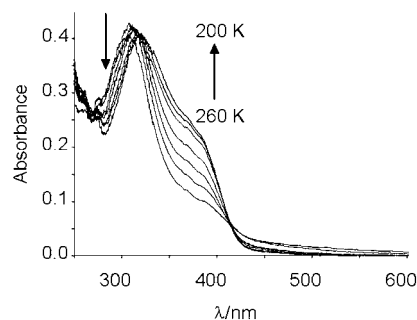


Figure 4. UV/Vis spectra taken at each 10 K interval between 200 and 260 K for a CH<sub>2</sub>Cl<sub>2</sub> solution containing PNP (0.001 M) and [Cp\*FeH(dppe)] (0.00033 M).

ther the free phenolate band, expected at 420–430 nm, nor the band of homoconjugated anion [ArOHOAr]<sup>−</sup>, expected at approximately 400 nm, is observed, suggesting that hydrogen-bonded ion pair essentially does not dissociate below 260 K. These qualitative observations are in agreement with the equilibria depicted in Scheme 2 (R = *p*-O<sub>2</sub>N-C<sub>6</sub>H<sub>4</sub>) and with the exothermicity for both the hydrogen bond formation and for the proton transfer steps.

The exothermicity of the hydrogen bond formation falls in line with the hydrogen bond strength previously determined with the MFE and TFE proton donors (−4.6 and −5.9 kcal mol<sup>−1</sup>, respectively) and with the fact that PNP has a proton donor ability and acidity (*P*<sub>i</sub> = 1.27<sup>[50]</sup> and *pK*<sub>a</sub> =

10.8<sup>[51]</sup> or 10.4<sup>[52]</sup> in DMSO) comparable to those of PFTB (*P*<sub>i</sub> = 1.33 and *pK*<sub>a</sub> = 10.7<sup>[51]</sup> in DMSO). Therefore, the strength of the hydrogen bonding interaction with PNP is expected to be even greater. The exothermicity of the proton transfer step is also in qualitative agreement with the thermodynamic parameters previously determined for the [Cp\*Fe(dppe)H]/HFIP system (see also later).

#### Interaction of [Cp\*FeH(dppe)] with the TFA: IR study:

The interaction of [Cp\*FeH(dppe)] with TFA was previously investigated kinetically, but the initial proton transfer is too fast to measure within the stopped-flow time constraints. Only the rate of isomerization of the intermediate dihydrogen complex was kinetically accessible, whereas the initial proton transfer is quantitative within the minimum time lapse for the first measurement (ca. 1 ms). Trifluoroacetate is a weaker base than *p*-nitrophenolate or [(CF<sub>3</sub>)<sub>2</sub>CHO]<sup>−</sup> and gives weaker bonding with the dihydrogen cation.<sup>[20]</sup> Although the trifluoroacetate anion is colorless preventing the use of UV/Vis spectroscopy, IR spectroscopy can be conveniently used in this case because the ν<sup>as</sup>(OCO) bands are sufficiently diagnostic of the hydrogen bonding state of the TFA anion. The IR spectrum in the carbonyl stretching region for a 2:1 [Cp\*FeH(dppe)]/TFA mixture is shown in Figure 5a. Two new bands at 1692 and 1713 cm<sup>−1</sup>, assigned respectively to the free and hydrogen-bonded [CF<sub>3</sub>COO]<sup>−</sup> ion, are observed. At the same time, the acid band at 1780 cm<sup>−1</sup> is completely consumed and the ν(FeH) band at 1840 cm<sup>−1</sup> has half the intensity of a stock solution with the same concentration. When using a fivefold excess of the acid, no bands attributable to the free anion or to the hydro-

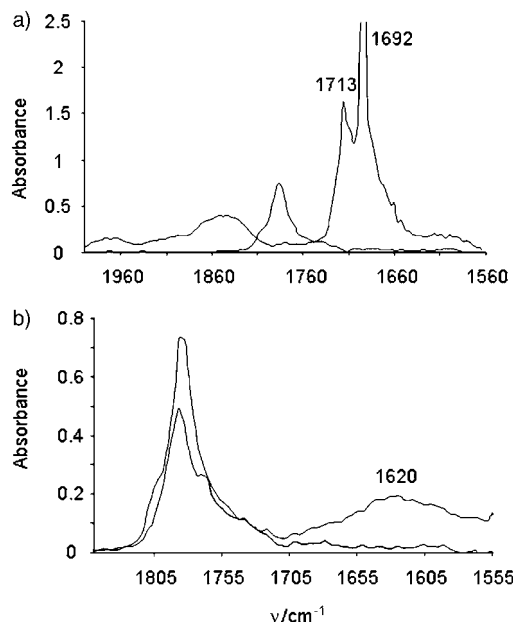


Figure 5. IR spectra at 200 K of CH<sub>2</sub>Cl<sub>2</sub> solutions containing [Cp\*FeH(dppe)] and TFA. a) [FeH] = 0.06 M, [TFA] = 0.03 M; b) [FeH] = 0.006 M, [TFA] = 0.03 M. The spectra of the solution containing only the free acid is also shown for comparison in both (a) and (b).

gen-bonded ion pair are visible (Figure 5b), whereas a wide and low intensity band is observed at  $1620\text{ cm}^{-1}$ . This corresponds to the free homoconjugated ion, in which the  $[\text{CF}_3\text{COO}]^-$  ion is bonded to two TFA molecules.<sup>[53]</sup> Evidently, since TFA is a much stronger acid, the initial hydrogen bond between TFA and the hydride complex is not observed because proton transfer occurs very rapidly and its equilibrium position leaves no measurable amounts of the hydride precursor in solution. On the other hand, the trifluoroacetate anion is a relatively weak base, being energetically stabilized by resonance. Thus, it is a weak proton acceptor for hydrogen bonding and consequently it is present in large proportions as the free base in solution, in equilibrium with the hydrogen-bonded base. In the presence of excess acid, the only carbonyl species present in solution are  $\text{CF}_3\text{COOH}$  and  $[\text{CF}_3\text{COO}(\text{HOCCF}_3)_2]^-$ .

**Interaction of  $[\text{Cp}^*\text{FeH}(\text{dppe})]$  with HFIP: thermodynamics of the hydrogen bond formation:** Our previous studies of hydrogen bonding were limited to the proton donors MFE and TFE, for which proton transfer does not occur at all or only very slowly at room temperature.<sup>[25]</sup> By carrying out IR studies in the  $\nu_{\text{OH}}$  region at low temperatures (200–280 K) according to our established protocol, we have now obtained the thermodynamic parameters for the  $[\text{Cp}^*\text{Fe}(\text{dppe})\text{H}]\text{--HFIP}$  hydrogen bonding interaction ( $\Delta H^\circ = -6.5 \pm 0.4\text{ kcal mol}^{-1}$ ,  $\Delta S^\circ = -18.6 \pm 1.7\text{ cal mol}^{-1}\text{ K}^{-1}$ ) (Figure 6). These parameters indicate stronger bonding for HFIP relative to TFE ( $\Delta H^\circ = -5.4 \pm 0.3\text{ kcal mol}^{-1}$  and  $\Delta S^\circ = -13.6 \pm 0.9\text{ cal mol}^{-1}\text{ K}^{-1}$ ),<sup>[25]</sup> as expected.

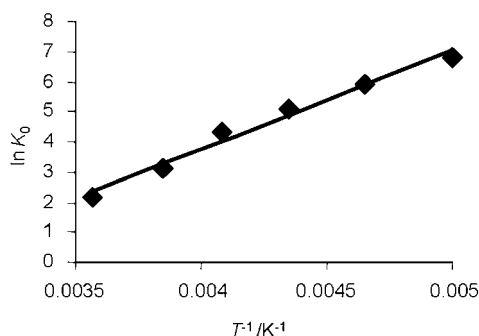
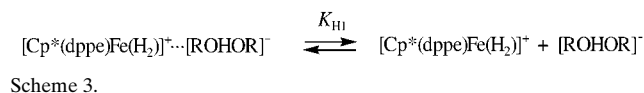


Figure 6. Equilibrium constant at different temperatures for hydrogen bond formation between  $[\text{Cp}^*\text{Fe}(\text{dppe})\text{H}]$  and HFIP.

The same investigation could not be carried out for the hydrogen bonding interaction with PNP, because this phenol (whose acidity and proton donor strength are close to those of PFTB as shown above) yields proton transfer processes, as is evident from the low-temperature UV/Vis spectra (e.g. see Figure 2).

**Interaction of  $[\text{Cp}^*\text{FeH}(\text{dppe})]$  with the HFIP: thermodynamics of the proton transfer equilibrium:** We have previously analyzed the proton transfer equilibrium for the  $[\text{Cp}^*\text{FeH}(\text{dppe})]$  with the HFIP system by UV/Vis spectro-

scopy, but the analysis did not take into account the hydrogen bonding equilibrium [ $K_{\text{H0}}$  in Scheme 2,  $\text{R} = (\text{CF}_3)_2\text{CH}$ ] for the starting material. The knowledge that is now available for this equilibrium (see previous section), allows us to recalculate the equilibrium and thermodynamic parameters for the proton transfer step. However, knowledge is still lacking about the hydrogen bonding equilibrium for the ionic dihydrogen complex product ( $K_{\text{H1}}$  in Scheme 3,  $\text{R} =$



$(\text{CF}_3)_2\text{CH}$ ). The hydrogen bond in the product ion pair is expected to be stronger relative to that of the neutral precursor, because of the stronger Coulombic component for the charge-separated species. Moreover  $[(\text{CF}_3)_2\text{CHO}]^-$  is a stronger base than *p*-nitrophenolate, for which no dissociation of the hydrogen-bonded ion pair was observed (see above). Thus, the product is likely to remain as a hydrogen-bonded ion pair in the relatively nonpolar dichloromethane solvent, especially in the low temperature range used for the equilibrium measurements (200–260 K). Under this hypothesis, the equilibrium  $K_{\text{H1}}$  may be neglected, yielding  $K_1 (=k_1/k_{-1})$ .

A van't Hoff analysis of the  $K_1$  constants derived from the previously published<sup>[25]</sup> UV/Vis data yields  $\Delta H = -5.5 \pm 0.3\text{ kcal mol}^{-1}$  and  $\Delta S = -13.0 \pm 0.6\text{ cal mol}^{-1}\text{ K}^{-1}$ . It is necessary to point out that, besides the neglect of the  $K_{\text{H1}}$  equilibrium, this analysis also makes use of the hypothesis of a temperature- and anion-independent UV/Vis spectrum for species  $[\text{Cp}^*(\text{dppe})\text{Fe}(\text{H}_2)]^+ \cdots [\text{ROHOR}]^-$  (see Experimental Section and Supporting Information).

An alternative way to analyze the proton transfer equilibrium is provided by NMR spectroscopy. Our previous contribution included  $^1\text{H}$  and  $^{31}\text{P}$  NMR investigations of the interaction between  $[\text{Cp}^*\text{FeH}(\text{dppe})]$  and ROH (TFE, HFIP, and PFTB),<sup>[25]</sup> but did not include the accurate measurement of the proton transfer equilibrium position as a function of temperature. The formation of the hydrogen bond occurs without an energy barrier, thus the NMR resonances of free and hydrogen-bonded hydride complexes are in the fast exchange regime at all temperatures, as are those of the dihydrogen complex  $[\text{Cp}^*\text{Fe}(\text{dppe})(\text{H}_2)]^+$  and that of its hydrogen-bonded adduct  $[\text{Cp}^*\text{Fe}(\text{dppe})(\text{H}_2)]^+ \cdots [\text{ROHOR}]^-$ , which are seen at  $\delta \approx -17.3$  and  $-12.5$  ppm in the  $^1\text{H}$  NMR spectrum and at  $\delta \approx 93.8$  and  $108$  ppm in the  $^{31}\text{P}$  NMR spectrum, respectively. The distinction of these two resonances, on the other hand, shows that the proton transfer equilibrium is in the slow exchange regime. The positions of these peaks do not shift significantly with temperature and with the nature or concentration of the proton donor. Thus, the chemical shifts cannot be used as indicators for the presence and extent of hydrogen bonding, neither for the starting



neutral hydride complex, nor for the cationic nonclassical complex.

The measured relative intensities of the significant resonances (hydride ligand resonance in the  $^1\text{H}$  NMR spectrum and phosphine resonance in the  $^{31}\text{P}$  NMR spectrum) yield the equilibrium concentration of the various species reported in Table 2, as detailed in the Experimental Section. The

readily established by the previous study, the hydrogen bond formations ( $K_{\text{H}_0}$  and  $K_{\text{H}_1}$ ) are instantaneous and equilibrated, the proton transfer step ( $k_1$ ,  $k_{-1}$ ; first measurable rate) is equilibrated and  $[\text{R}_\text{F}\text{OH}]$ -dependent, whereas the internal rearrangement from dihydrogen complex to classical dihydride ( $k_2$ ; second measurable rate) is irreversible and  $[\text{R}_\text{F}\text{OH}]$ -independent.

Table 2. Concentrations of different species as a function of temperature from the  $^1\text{H}$  and  $^{31}\text{P}$  NMR study of the reaction between  $[\text{Cp}^*\text{FeH}(\text{dppe})]$  and HFIP.<sup>[a]</sup>

$T$	$^1\text{H}$ spectra				$^{31}\text{P}$ spectra			
	$[\text{FeH}]^{[b]}$	$[\text{FeH}\cdots\text{H}]^{[c]}$	$[\text{Fe}(\text{H}_2)]^{[d]}$	$K_1$	$[\text{FeH}]^{[b]}$	$[\text{FeH}\cdots\text{H}]^{[c]}$	$[\text{Fe}(\text{H}_2)]^{[d]}$	$K_1$
220	0.0323	0.0224	0.0127	125.17	0.0343	0.0204	0.0141	171.33
240	0.0373	0.0174	0.0120	72.58	0.0379	0.0168	0.0126	82.28
250	0.0393	0.0154	0.0109	55.10	0.0397	0.0150	0.0114	60.16
260	0.0411	0.0136	0.0095	41.31	0.0411	0.0136	0.0096	41.80
270	0.0430	0.0117	0.0082	32.82	0.0431	0.0116	0.0084	34.30

[a]  $C_{\text{Fe}} = C_{\text{HFIP}} = 0.0547 \text{ M}$ . [b]  $[\text{FeH}] = [\text{Cp}^*\text{Fe}(\text{dppe})\text{H}]$ . [c]  $[\text{FeH}\cdots\text{H}] = [\text{Cp}^*\text{Fe}(\text{dppe})\text{H}\cdots\text{HOR}]$ . [d]  $[\text{Fe}(\text{H}_2)] = ([[\text{Cp}^*\text{Fe}(\text{dppe})(\text{H}_2)]^+ + [[\text{Cp}^*\text{Fe}(\text{dppe})(\text{H}_2)]^+\cdots[\text{ROHOR}^-]])$ .

experiment cannot give equilibrium data at temperatures above 270 K, because of the incipient isomerization to the classical dihydride product. We should mention here that the resonances of the neutral hydride complex were previously reported to broaden extensively as the temperature was raised, a phenomenon that was attributed to a fast self-exchange with the adventitious product of one-electron oxidation.<sup>[25]</sup> The present experiment was carried out on a recrystallized, pure sample and under rigorous conditions. The measured  $^1\text{H}$  NMR resonance for the neutral hydride complex was sharp, with a well-resolved P coupling and much longer  $T_1$  values relative to the previous report.

As Table 2 shows, the integration of both the  $^1\text{H}$  and the  $^{31}\text{P}$  data leads to very similar concentration data. Again, under the assumption that the  $K_{\text{H}_1}$  equilibrium favors the hydrogen-bonded adduct quantitatively (i.e.  $[\text{Fe}(\text{H}_2)]$  in Table 2 corresponds to the concentration of the hydrogen bonded species,  $[[\text{Cp}^*\text{Fe}(\text{dppe})(\text{H}_2)]^+\cdots[\text{ROHOR}^-]]$ ), the derived values of  $K_1$  in Table 2 correspond to the true equilibrium constant for the proton transfer process,  $k_1/k_{-1}$ . The van't Hoff analysis on  $K_1$  yields  $\Delta H_1 = -3.2 \pm 0.1 \text{ kcal mol}^{-1}$  and  $\Delta S_1 = -4.8 \pm 0.4 \text{ cal mol}^{-1} \text{ K}^{-1}$  from the  $^1\text{H}$  NMR data;  $\Delta H_1 = -3.9 \pm 0.1 \text{ kcal mol}^{-1}$  and  $\Delta S_1 = -7.4 \pm 0.4 \text{ cal mol}^{-1} \text{ K}^{-1}$  from the  $^{31}\text{P}$  NMR data. These values are rather close to those established from the low-temperature UV/Visible data. Averages of the values obtained with the three different methods are:  $\Delta H_1 = -4.2 \pm 1.2 \text{ kcal mol}^{-1}$ ;  $\Delta S_1 = -8 \pm 4 \text{ cal mol}^{-1} \text{ K}^{-1}$ .

**Interaction of  $[\text{Cp}^*\text{FeH}(\text{dppe})]$  with the HFIP: proton transfer activation barrier:** The proton transfer from HFIP to  $[\text{Cp}^*\text{FeH}(\text{dppe})]$  has been investigated by the stopped-flow method in the temperature range 288–308 K. Our previous kinetic investigation of this process was limited to room temperature.<sup>[25]</sup> The transformation consists of the establishment of the proton transfer equilibrium, followed by the rearrangement to the classical dihydride product. As al-

The values of  $k_1$  and  $k_{-1}$  were previously obtained from the slope and the intercept of the  $k_{\text{obs}}$  versus  $[\text{R}_\text{F}\text{OH}]$  plot for each alcohol. We have now taken a more rigorous approach, consisting of the use of the complete model  $\text{A} \rightarrow \text{B}$  ( $k_{1\text{obs}}$ ),  $\text{B} \rightarrow \text{A}$  ( $k_{-1\text{obs}}$ ) and  $\text{B} \rightarrow \text{C}$  ( $k_2$ ). The use of SPECFIT<sup>[28]</sup> allows in principle the independent determination of the values of the three rate constants for each experiment. The A kinetic species is the equilibrium mixture of free and hydrogen-bonded  $[\text{Cp}^*\text{Fe}(\text{dppe})\text{H}]$ , whereas B and C are the equilibrium mixtures of free and hydrogen-bonded intermediate dihydrogen complex and final dihydride product, respectively. The expression relating the observed rate constant  $k_{1\text{obs}}$  to the true rate constants  $k_1$  and the equilibrium constant  $K_{\text{H}_0}$  is given in Equation (3). The value of  $k_{-1\text{obs}}$  corresponds to  $k_{-1}$  under the above approximation of quantitative formation of the  $[\text{Cp}^*\text{Fe}(\text{dppe})(\text{H}_2)]^+\cdots[\text{ROHOR}]^-$  hydrogen bond.

$$k_{1\text{obs}} = \frac{k_1 K_{\text{H}_0} [\text{ROH}]^2}{(1 + K_{\text{H}_0} [\text{ROH}])} \quad (3)$$

This analysis method has the advantage of not requiring the use of different ROH concentrations at each temperature to determine the individual rate constants. However, the analysis requires precise knowledge of the spectrum of the intermediate species B. In fact, the three rate constants are highly correlated with each other and with the position of the proton transfer equilibrium, thus equally excellent data fits result from analyses carried out with different B spectra that reflect different equilibrium situations. The correct fit is only obtained if the B spectrum is that of the pure dihydrogen complex. Of course, this intermediate species cannot be generated in solution in a pure state, in the presence of the same counterion and under the same temperature conditions of the kinetic measurement. To circumvent this problem, we have generated several different solutions of the "pure" dihydrogen complex under different conditions and recorded their spectra, and we also constructed spectra of the pure complex with the same counterion (see Supporting Information). Consistent results were obtained by using five different spectra, but only limited to the activation parameters related to the forward rate constant  $k_1$ . The most reliable results are believed to be  $\Delta H^\ddagger_1 = 2.6 \pm 0.3 \text{ kcal mol}^{-1}$  and  $\Delta S^\ddagger_1 = -44.5 \pm 1.1 \text{ cal mol}^{-1} \text{ K}^{-1}$ .<sup>[54]</sup> The

full set of results is available as Supporting Information. The activation parameters for the  $k_{-1}$  and  $k_2$  steps turned out to be extremely sensitive to the nature of the B spectrum. Their discussion is not warranted here (see Supporting Information). The activation parameters for the reverse proton transfer step ( $k_{-1}$ ) may be more appropriately estimated from the independent knowledge of the activation parameters of the forward step plus the equilibrium parameters obtained from the UV/Vis or NMR studies (see previous section). The activation parameter for the isomerization step ( $k_2$ ) will be measured independently and more accurately using a stronger proton donor, and the results will be reported in a separate contribution.<sup>[26]</sup>

In conclusion, the combination of the various techniques used to investigate the interaction between  $[\text{Cp}^*\text{Fe}(\text{dppe})\text{H}]$  and HFIP, to yield  $[\text{Cp}^*\text{Fe}(\text{dppe})(\text{H}_2)]^+$  and  $[\text{ROHOR}]^-$  ( $\text{R}=(\text{CF}_3)_2\text{CH}$ ), affords the following information: 1) the equilibrated proton transfer process occurs starting from the hydrogen-bonded adduct  $[\text{Cp}^*\text{Fe}(\text{dppe})\text{H}]\cdots\text{HOR}$  only after intervention of a second ROH molecule and leads to the hydrogen-bonded adduct  $[\text{Cp}^*\text{Fe}(\text{dppe})(\text{H}_2)]^+\cdots[\text{ROHOR}]^-$ ; 2) this product equilibrates with the free ions but this equilibrium most probably lies on the side of the hydrogen bonded ion pair, at least in dichloromethane at low temperatures; 3) the proton transfer process is exothermic ( $\Delta H^\circ$  between  $-3$  and  $-5$  kcal mol $^{-1}$ ) and with a negative entropy ( $\Delta S^\circ$  between  $-5$  and  $-13$  cal mol $^{-1}$  K $^{-1}$ ); 4) the proton transfer has a low activation enthalpy ( $2.6 \pm 0.3$  kcal mol $^{-1}$ ) and a very negative activation entropy ( $-44.5 \pm 1.1$  cal mol $^{-1}$  K $^{-1}$ ).

**Theoretical study:** Theoretical calculations have been carried out on the reaction between models of the  $[\text{Cp}^*\text{Fe}(\text{dppe})\text{H}]$  complex and different proton donors HA to highlight some of the governing factors of each step of the protonation reaction.<sup>[20]</sup> The presentation of the theoretical results is divided in two parts. The first one will be devoted to the thermodynamics of the formation of the initial hydrogen-bonded complexes, both in the gas phase and in dichloromethane (DCM). In the second part, we will focus on the thermodynamics and the kinetics of the proton transfer process converting the hydrogen-bonded complexes to the ion pair. The solvent and the homoconjugated pairing effects are also discussed in this section.

**Determination of the hydrogen bonding site:** We have considered the interaction of the  $[\text{Cp}^*\text{Fe}(\text{dhpe})\text{H}]$  ( $\text{dhpe} = \text{H}_2\text{PCH}_2\text{CH}_2\text{PH}_2$ ) model complex with the following set of proton donors of increasing acidity:  $\text{MFE} < \text{TFE} < \text{HFIP} < \text{PFTB} < \text{TFA}$ , that is, the proton donors that were used in our previous experimental investigation.<sup>[25]</sup> The formation of the hydrogen bond was investigated at both the hydride and metal sites. The optimized geometries of the hydrogen-bonded adducts are presented in Figure 7 with the associated parameters in Table 3.

The geometrical parameters that describe the hydrogen bond are quite similar to those computed previously<sup>[20]</sup> for

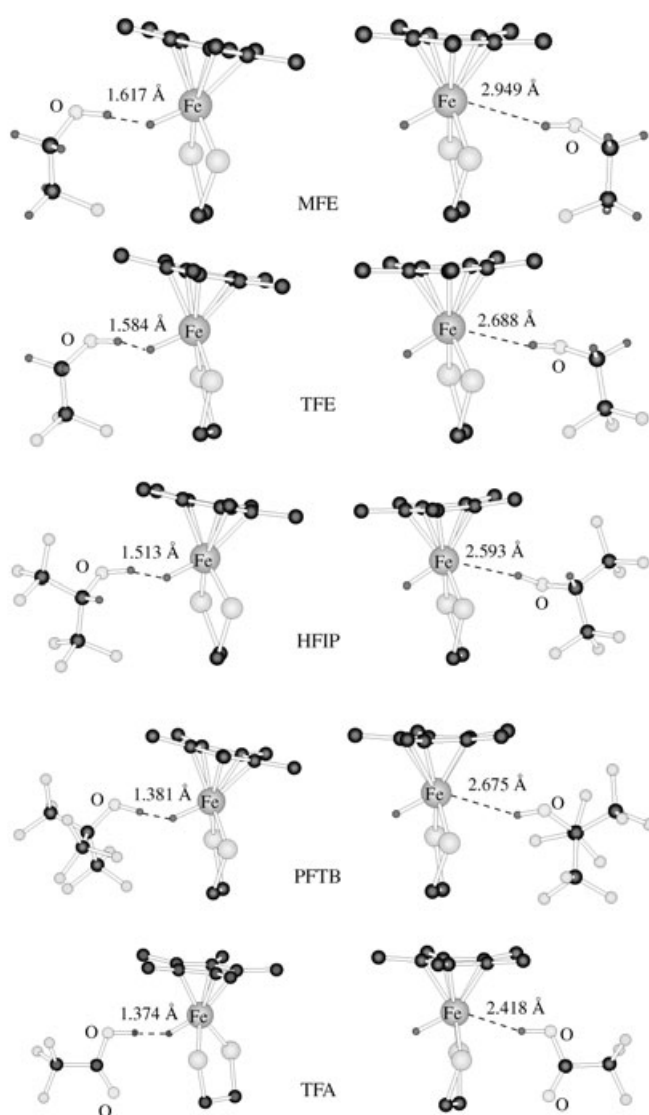


Figure 7. Optimized geometries of the hydrogen-bonded adducts at the hydride and metal sites with the set of proton donors. Hydrogen atoms (except for those involved in the hydrogen bond) are omitted for clarity.

$[\text{CpRuH}(\text{CO})(\text{PH}_3)]$ , as a model of the  $[\text{CpRuH}(\text{CO})(\text{PCy}_3)]$  complex, interacting with moderate proton donors. The computed dihydrogen bonds ( $\text{AH}\cdots\text{HFe}$ ) are slightly shorter than those reported for the  $[\text{CpRuH}(\text{CO})(\text{PH}_3)]$  model complex due to the higher basicity of  $[\text{Cp}^*\text{Fe}(\text{dppe})]$  ( $E_i = 1.35$  for  $[\text{Cp}^*\text{Fe}(\text{dppe})\text{H}]$ <sup>[25]</sup> compared to  $E_i = 1.02$  for  $[\text{CpRuH}(\text{CO})(\text{PCy}_3)]$ <sup>[12]</sup>). The formation of the hydrogen bonds is reflected in the lengthening of the OH bond lengths ( $\Delta d(\text{OH})$ ) from their values in the isolated proton donors and consequently by the shift of  $\nu(\text{O}-\text{H})$ , see Table 3. Note that  $\Delta d(\text{OH})$  is greater for the hydride site, signaling stronger bonding. The binding of the proton donors at the hydride site also produces a Fe-H bond lengthening, which follows the order of the acidic strength of the proton donor. On the other hand, the Fe-H bond is slightly shortened by the binding at the metal site.



Table 3. Parameters describing the hydrogen-bonding interaction at the hydride and metal sites for complex [Cp\*Fe(dhpe)H].

HA		$d(\text{H}\cdots\text{X})^{[a]}$ [Å]	$\Delta d(\text{Fe}-\text{H})^{[b]}$ [Å]	$\Delta d(\text{O}-\text{H})^{[b]}$ [Å]	$\Delta \nu(\text{O}-\text{H})^{[b]}$ [cm <sup>-1</sup> ]	$\Delta E_{\text{Gas}}^{[c]}$ [kcal mol <sup>-1</sup> ]	$\Delta E_{\text{Gas BSSE}}^{[d]}$ [kcal mol <sup>-1</sup> ]	$\Delta G_{\text{DCM}}^{[e]}$ [kcal mol <sup>-1</sup> ]	$\Delta H^{\circ [f]}$ [kcal mol <sup>-1</sup> ]
MFE	H $\cdots$ H <sup>[g]</sup>	1.617	0.007	0.016	-330	-10.6	-6.1	-3.7	-5.7
	H $\cdots$ Fe <sup>[h]</sup>	2.949	-0.004	0.006	-122	-6.8	0.2	-0.7	-2.6
TFE	H $\cdots$ H <sup>[g]</sup>	1.584	0.012	0.021	-432	-12.2	-6.1	-4.1	-6.8
	H $\cdots$ Fe <sup>[h]</sup>	2.688	-0.004	0.012	-257	-7.2	-1.0	0.7	-4.8
HFIP	H $\cdots$ H <sup>[g]</sup>	1.513	0.016	0.027	-571	-13.8	-7.4	-4.2	-8.0
	H $\cdots$ Fe <sup>[h]</sup>	2.593	-0.005	0.015	-361	-8.1	-0.9	1.2	-6.0
PFTB	H $\cdots$ H <sup>[g]</sup>	1.381	0.014	0.045	-898	-14.3	-7.6	-3.7	-10.0
	H $\cdots$ Fe <sup>[h]</sup>	2.675	-0.006	0.017	-353	-7.2	0.6	3.6	-7.0
TFA	H $\cdots$ H <sup>[g]</sup>	1.374	0.015	0.048	-954	-14.5	-10.7	-5.9	-10.4
	H $\cdots$ Fe <sup>[h]</sup>	2.418	-0.007	0.021	-701	-9.1	-4.3	-0.1	-8.9

[a] X = (H, Fe). [b] Difference between the value in the free compounds and in the hydrogen-bonded adduct. [c] Complexation energy in the gas phase. [d] Complexation energy in the gas phase corrected by the basis set superposition error. [e] Complexation free energy in dichloromethane. [f] Enthalpy of the hydrogen bond formation from Iogansen's empirical rule.<sup>[55]</sup> [g] Hydride site. [h] Metal site.

The energy changes associated with the hydrogen bond formation are more negative for the hydride site than for the metal site for all the proton donors (Table 3). This trend is observed both in the gas phase and in DCM.  $\Delta G$  values at the metal site are positive for TFE, HFIP and PFTB, and very slightly negative for MFE and TFA, meaning that the corresponding hydrogen-bonded complexes presumably do not exist in solution. The gas phase complexation energies of the different proton donors at the hydride site follow the acidic strength order. The same trend is found at the Fe site, except for the PFTB molecule. In comparison with the other proton donors, PFTB is a quite bulky molecule due to the three CF<sub>3</sub> groups, preventing the PFTB from easily reaching the Fe site. The complexation energies are in the same range as those obtained for the same kind of interactions in other hydride systems.<sup>[56–58]</sup>

The hydrogen bond formation enthalpies,  $\Delta H^{\circ}$ , reported in Table 3 are calculated by means of the Iogansen's empirical rule,<sup>[55]</sup> using the computed OH frequency shifts. There is rather good agreement between the computed hydrogen bonding enthalpies and those obtained from the IR experiments ( $-4.6$  kcal mol<sup>-1</sup> for MFE,  $-5.9$  kcal mol<sup>-1</sup> for TFE).<sup>[25]</sup> Our computed  $\Delta H^{\circ}$  values are slightly more negative, possibly because the experimental values are obtained in dichloromethane solvent whereas the frequency calculations were carried out in the gas phase where the interaction between the proton donor and the [Cp\*Fe(dhpe)H] complex is stronger. As expected, the more acidic the proton donor, the stronger the interaction (as reflected by more negative values of  $\Delta H^{\circ}$ ). This is in agreement with the experimental trends of  $\Delta H^{\circ}$  for MFE, TFE and HFIP. In addition, bonding energies corrected by the basis set superposition error (BSSE) have been also calculated because previous results concerning M–H $\cdots$ H–OR hydrogen bonds showed that the BSSE can be very important in this type of system.<sup>[59]</sup> Indeed, the BSSE energy can be up to 50% of the interaction energy both at the hydride

and the metal site. Consequently, the BSSE-corrected energies at the hydride site are close to the enthalpies of formation of the hydrogen bond. At the metal site, the BSSE causes the complexation energies to be close to zero or even positive, meaning that the BSSE is the main component of the complexation energies. These first computational results identify the hydride site of the [Cp\*Fe(dhpe)H] complex as the initial bonding site for all proton donors prior to the proton transfer process, in agreement with the experimental results on the [Cp\*Fe(dppe)H] complex.<sup>[25]</sup>

We have checked the suitability of the model used above by carrying out additional calculations on different models of the iron complex with TFE as proton donor (Table 4).

Table 4. Gas phase hydrogen bond energies (in kcal mol<sup>-1</sup>) at hydride and metal sites with TFE for different models of the real [Cp\*Fe(dppe)H] complex.

	[CpFe(dhpe)H] B3LYP	[Cp*Fe(dhpe)H] B3LYP	[Cp*Fe(dppe)H] IMOMM	[Cp*Fe(dppe)] IMOMM/B3LYP <sup>[a]</sup>
$\Delta E_{\text{Gas H}\cdots\text{H}}$	-10.6	-12.2	-12.8	-12.3
$\Delta E_{\text{Gas H}\cdots\text{Fe}}$	-7.5	-7.2	-4.4	-3.2

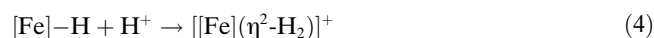
[a] Interaction energies computed at the B3LYP level on the IMOMM optimized geometries.

Whatever the model used, the complexation energy is always more negative at the hydride site than at the metal site. At the hydride site, going from [CpFe(dhpe)H] to [Cp\*Fe(dhpe)H], the complexation energy is slightly more negative because the electron richer Cp\* ligand enhances the basicity of the hydride ligand. Adding the phenyl to the P atoms at a molecular mechanics level does not change the energy in a significant way, meaning that there is no steric hindrance at the hydride site caused by the phenyl groups. In fact, the Cp\* is slightly tilted away from the hydride site and the access to the proton acceptor site is consequently easier at the hydride than at metal site (see Figure 7). To introduce the electronic effects of the phenyl substituents while keeping the computation affordable, B3LYP interaction energies on the real [Cp\*Fe(dppe)H] system have been calculated by means of full quantum-mechanical single-point calculations at the IMOMM optimized geometries. The reliability of such an approach has been discussed previ-

ously.<sup>[60,61]</sup> The interaction energy at the hydride site remains almost unchanged, showing that the electronic effect of the phenyl substituents is also small. The results at the metal site contrast with those at the hydride site. [CpFe(dhpe)H] and [Cp\*Fe(dhpe)H] model complexes lead to comparable energies, but adding phenyl ligands at the IMOMM level decreases the interaction energy considerably. This highlights the steric hindrance caused by the phenyl substituents of the dppe ligand when the proton donor comes close to the metal site. The electronic effects of the phenyl groups, on the other hand, seem less important than for the case of the hydride site, as shown by the similar values of the IMOMM and IMOMM/B3LYP interaction energies.

As a conclusion of this calibration study, [Cp\*Fe(dhpe)H] seems a good model of the real system for what concerns the interaction energies at the hydride site, whereas it overestimates the interaction energies at the metal site. This is mainly due to the neglect of the steric effects introduced by the phenyl substituents.

**Proton transfer for TFA and HFIP:** In some of the proton transfer investigations we shall use a system comprising two proton donor molecules, in line with the experimental results of the kinetics study and with previous computations on other systems.<sup>[20]</sup> This considerably enlarges the size of the system. Therefore, for computational limitation and in order to keep the computation affordable, we have only considered the [CpFe(dhpe)H] model in this part. However, we have first carried out test computations to check how the computational level and the chosen model affect the gas phase hydride proton affinity (PA), that is, the energy change involved in Equation 4, for the monohydride iron complex. The results are reported in Table 5.



The B3LYP level of computation with the basis set used appears suitable for our purpose. CCSDT proton affinities are close to the B3LYP results. The effect of adding polarization functions to the carbon atoms of the Cp can be considered as unimportant because the values only change by about 1.0 kcal mol<sup>-1</sup>. The proton affinity increases on going from the simplest to the largest models. Substitution of Cp by the more basic Cp\* ligand increase the PA by 8.6 kcal mol<sup>-1</sup>. The electronic effect of the phenyl substituents further increases the PA by a similar amount (8.6 kcal mol<sup>-1</sup>). The model system adopted presents a slightly lower proton affinity than the real system, but the difference amounts to only 7%.

Table 5. Proton affinity of the monohydride complex

	Proton affinity [kcal mol <sup>-1</sup> ]
[CpFe(dhpe)H]/B3LYP	250.1 (251.1 <sup>[a]</sup> )
[CpFe(dhpe)H]/CCSDT <sup>[b]</sup>	255.1
[Cp*Fe(dhpe)H]/B3LYP	258.7 (259.4 <sup>[a]</sup> )
[Cp*Fe(dppe)H]/IMOMM	256.5
[Cp*Fe(dppe)H]/B3LYP	267.1

[a] Computed by adding polarization functions on the carbon atoms of the Cp ring. [b] Single-point CCSDT computation on DFT/B3LYP-optimized geometries.

**TFA:** Starting from the hydrogen-bonded adducts presented in the previous section (Figure 7) we have studied the proton transfer process both to the hydride and to the metal site. We started by optimizing the geometry of the final products: the ion pair comprising the dihydrogen complex (protonation at the hydride site) or dihydride complex (protonation at the metal site) and [CF<sub>3</sub>COO]<sup>-</sup>.

In the gas phase, both ion pairs are found as minima (Figure 8). In the optimized structures the O...H separations are 2.053 Å and 1.849 Å at hydride and metal site, respectively. The proton transfer therefore seems more accom-

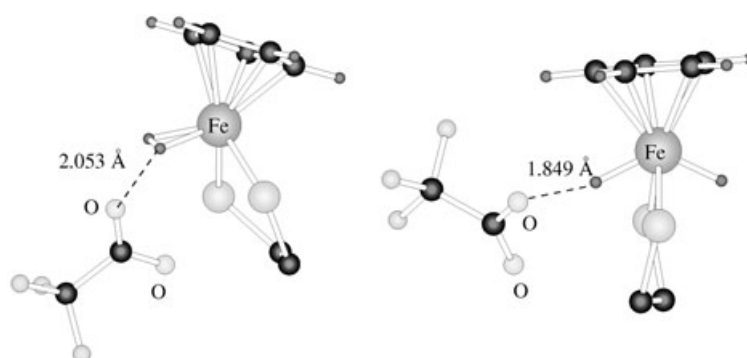


Figure 8. Optimized geometries of the [[Fe]-“H<sub>2</sub>”]<sup>+</sup>...[OOCF<sub>3</sub>]<sup>-</sup> ion pairs. Left: protonation at the hydride site; right: protonation at the metal site. Hydrogen atoms of PH<sub>2</sub>CH<sub>2</sub>CH<sub>2</sub>PH<sub>2</sub> are not displayed.

plished at the hydride site, highlighting the stronger basicity of the hydride ligand relative to the metal. One must notice that ion pairs were previously reported as stable structures along the pathway to the protonation of metal hydrides only when a second molecule of a moderate proton donor was involved in the transfer, by the homoconjugated pairing effect.<sup>[20]</sup> Here, a second proton donor molecule is not required to obtain a stable ion pair. This is in good agreement with the experimental result when protonation of the [Cp\*Fe(dppe)H] complex is carried out with a low concentration of TFA (see next section).

Figure 9 reports the energetic profile for the proton transfer from one molecule of TFA to [CpFe(dhpe)H]. The O-H bond length of the TFA donor has been chosen as the reaction coordinate. All the other geometrical parameters were optimized for each fixed value of the reaction coordinate. The profiles in DCM solvent were obtained from single-point calculations on each point of the gas phase profiles with the PCM continuum model of the solvent. The energy

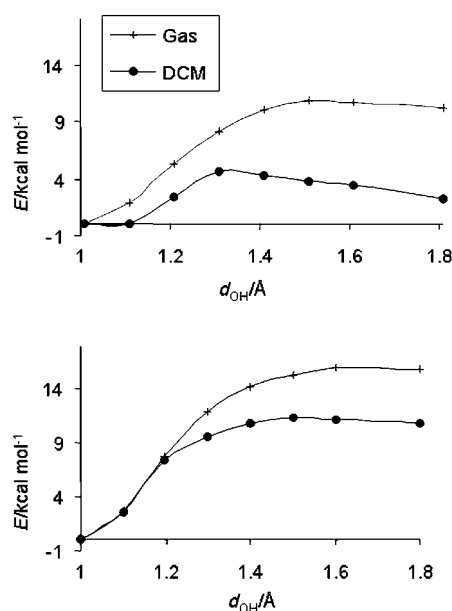


Figure 9. Potential energy curves for the proton transfer from one TFA molecule to complex [CpFe(dppe)H] at the hydride (top) and metal (bottom) sites. The O-H length of the transferring proton is the reaction coordinate. Energies are in  $\text{kcal mol}^{-1}$ .

of the dihydrogen-bonded adduct was taken as the zero of energy.

The gas-phase energy barriers to form the ion pair at the hydride site and at the metal site are 10.9 and 16.0  $\text{kcal mol}^{-1}$ , respectively. In DCM solvent the corresponding values are 4.6  $\text{kcal mol}^{-1}$  and 11.3  $\text{kcal mol}^{-1}$ . The kinetic effect of the solvent is to lower the energy barriers in comparison to the gas phase. The ion pairs resulting from the protonation at the hydride and metal site are found to be 10.2 and 15.8  $\text{kcal mol}^{-1}$ , respectively, above the hydrogen-bonded complexes in the gas phase, and at 2.2 and 10.8  $\text{kcal mol}^{-1}$  in DCM. We can see that there is also a thermodynamic effect of the solvent, stabilizing the charged species to a greater extent than the initial neutral hydrogen-bonded ones. Both solvent effects (kinetic and thermodynamic) are more pronounced for protonation at the hydride site, in good agreement with the experimental evidence that proton transfer takes place at the hydride site to form the ion pair with the nonclassical [Cp\*Fe(dppe)( $\eta^2\text{-H}_2$ )]<sup>+</sup> ion pair prior to the dihydrogen-dihydride isomerization.

We have also computed the energy profile of the proton transfer with a second TFA molecule assisting protonation by homoconjugated pairing. This situation can be related to experiments with an excess of TFA. The resulting [Fe(H<sub>2</sub>)]<sup>+</sup>...[OC(CF<sub>3</sub>)O...HOCCF<sub>3</sub>]<sup>-</sup> ion pairs are also found as minima. The ion pairs together with the initial dihydrogen bonded complexes are depicted in Figure 10.

In the initial hydrogen-bonded adducts with two TFA molecules, the latter are joined by a O...H hydrogen bond, with O-H separations of 1.735 Å and 1.773 Å for the hydride and Fe bonded adducts, respectively. In the two corresponding ion pairs there is a strong hydrogen bond in the

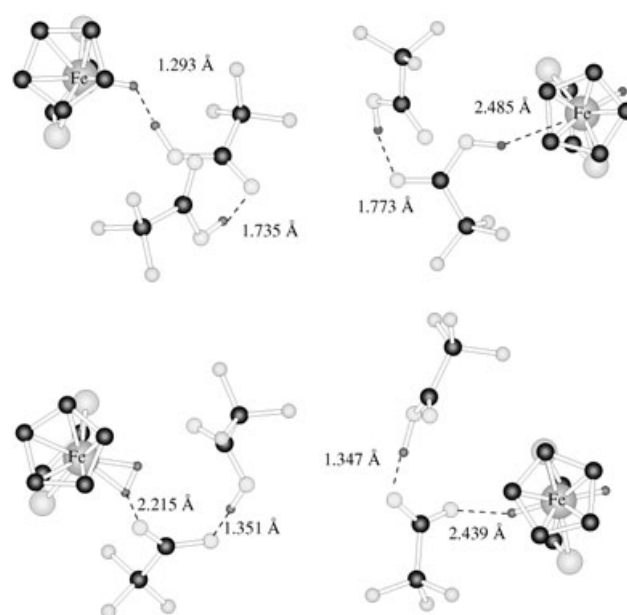


Figure 10. Top view of the optimized geometries of hydrogen-bonded complexes (top) and of the ion pair (bottom) with two TFA molecules. Left: hydride site protonation; right: metal site protonation. Hydrogen atoms of Cp and PH<sub>2</sub>CH<sub>2</sub>CH<sub>2</sub>PH<sub>2</sub> are not displayed.

homoconjugated pair, with similar intermolecular hydrogen bond length (1.351 Å and 1.347 Å, respectively). However, the O...H separation between the homoconjugated anion and the cationic [CpFe(dppe)H<sub>2</sub>]<sup>+</sup> is shorter at the hydride site (2.215 Å) than at the metal site (2.439 Å) reflecting the greater basicity of the former. Moreover, these values are longer than those computed with a single molecule of CF<sub>3</sub>COOH, showing that the second molecule enhances the acidity and favors the proton release.

Figure 11 reports the energetic profile of the proton transfer process to [CpFe(dppe)H] involving two hydrogen-bonded TFA molecules. The role of the second TFA molecule is to provide extra stabilization, through a strong hydrogen bond, to the [CF<sub>3</sub>COO]<sup>-</sup> base left over after the proton release, thereby reducing its basicity. The same effect was reported for the protonation of [CpRuH(CO)(PCy<sub>3</sub>)]<sup>[20]</sup> and [Cp\*Fe(dppe)H]<sup>[25]</sup> by weaker proton donors at the experimental and computational levels. There is a low energy barrier of about 3.0  $\text{kcal mol}^{-1}$  to be overcome to form the protonated dihydrogen complex in the gas phase, and this completely vanishes in CH<sub>2</sub>Cl<sub>2</sub>, meaning that this is quite an easy process. This result is in good agreement with experiment, because the proton transfer is very fast for TFA and the associated rate constant could not be estimated.<sup>[25]</sup> Moreover, as the solvent stabilizes the charge-separated proton transfer product to a greater extent than the neutral hydrogen-bonded complex, the process is more exothermic in dichloromethane than in the gas phase.

The situation is quite different when considering protonation at the Fe site. The potential energy curve for protonation exhibits a barrier of approximately 4.2  $\text{kcal mol}^{-1}$  in the gas phase, slightly higher than that for the protonation at

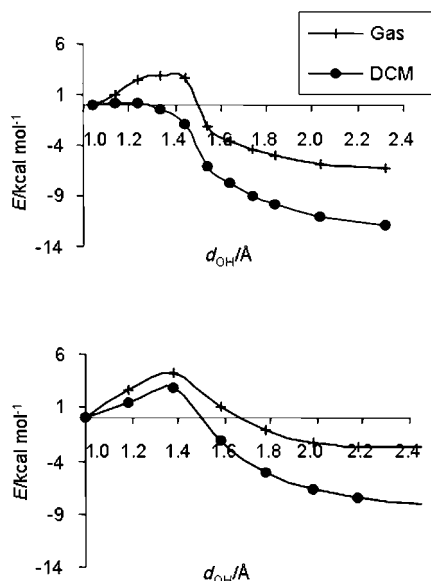


Figure 11. Potential energy curves for the proton transfer from two TFA molecules to the Fe complex at the hydride (top) and metal (bottom) sites. The O–H length of the transferring proton has been taken as the reaction coordinate. Energies are in kcal mol<sup>-1</sup>.

the hydride site. However, a barrier of 3.1 kcal mol<sup>-1</sup> still remains when adding the solvent effect. The kinetics of the proton transfer are consequently enhanced by the dichloromethane solvent only at the hydride site as we have found previously for the protonation with a single molecule of TFA. On the whole, our theoretical results confirm that the protonation is favored at the hydride site. In conclusion, the results show that there is a correlation between the thermodynamics of the hydrogen bond and the proton transfer kinetics for the two sites.

**HFIP:** We have performed the same computations reported above for the protonation process with HFIP because both kinetic and thermodynamic data are experimentally available. Attempts to optimize ion pairs related to proton transfer (at hydride and at metal sites) always failed when considering only one molecule of HFIP, the system going back to the initial hydrogen bonded complexes without exception. As HFIP is a weaker acid than TFA, its conjugate base is consequently stronger than [CF<sub>3</sub>COO]<sup>-</sup>. The [(CF<sub>3</sub>)<sub>2</sub>CHO]<sup>-</sup> ion is a stronger base than the [CpFe(dhpe)H] complex preventing the loss of one proton. For HFIP, a second molecule is needed to localize the ion pair as a minimum, by the homoconjugate pairing effect. One may remark that, for HFIP, the same oxygen atom of one conjugate base is involved in two hydrogen bonds (Figure 12) in comparison to TFA where one oxygen atom is involved in hydrogen bonding with the homoconjugate acid and the other one with the protonated complex (Figure 10). The O...H bond lengths between the homoconjugated anion and the protonated complex are respectively 1.807 Å and 2.031 Å at the hydride and the metal sites reflecting a stronger interaction in the former

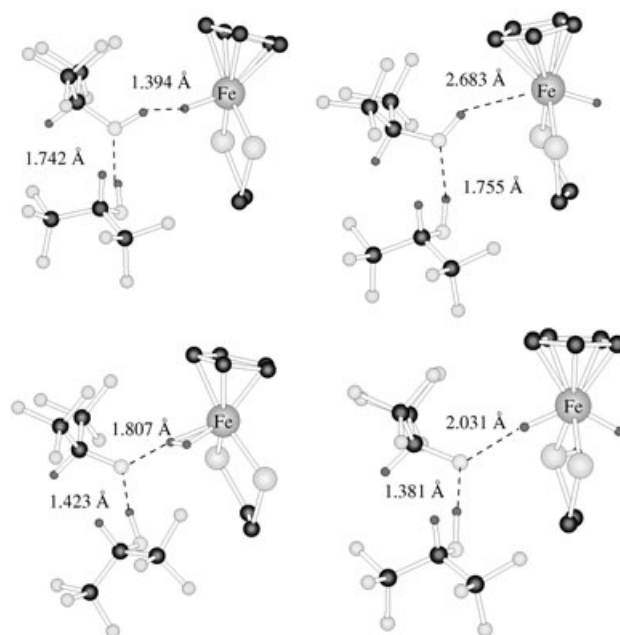


Figure 12. Optimized geometries of hydrogen-bonded complexes (top) and of the ion pair (bottom) with two HFIP molecules. Left: hydride site protonation; right: metal site protonation. Hydrogen atoms of Cp and PH<sub>2</sub>CH<sub>2</sub>CH<sub>2</sub>PH<sub>2</sub> are not displayed.

case. Conversely, hydrogen bonding with the proton of the second alcohol molecule is stronger in the latter case (1.423 Å and 1.381 Å, respectively).

The potential energy curves of the proton transfer with the two HFIP molecules (Figure 13) point out the same general solvent effects as found with TFA. At the hydride site, the energy barrier to formation of the ion pair in dichloro-

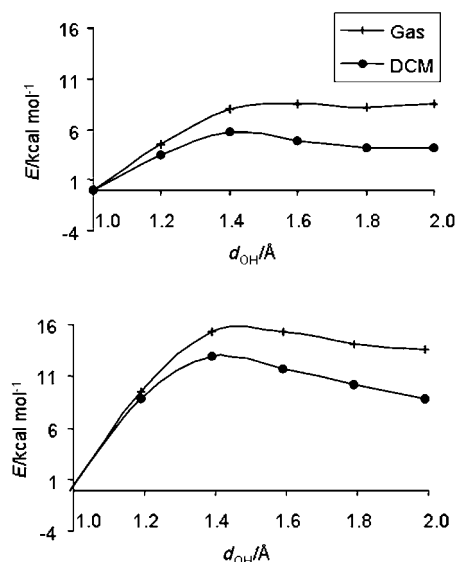


Figure 13. Potential energy curves for the proton transfer from two HFIP molecules to the Fe complex at the hydride (top) and metal (bottom) sites. The O–H length of the transferring proton has been taken as the reaction coordinate. Energies are in kcal mol<sup>-1</sup>.

methane ( $5.6 \text{ kcal mol}^{-1}$ ) is lower than in the gas phase ( $8.7 \text{ kcal mol}^{-1}$ ), illustrating the kinetic effect of the dichloromethane solvent. The proton transfer step with two HFIP molecules appears as an endothermic process by  $4.2 \text{ kcal mol}^{-1}$ . Concerning the proton transfer at the metal site, the solvent lowers the energy barrier found in the gas phase. However, a barrier of  $12.9 \text{ kcal mol}^{-1}$ , more than twice that for the protonation at the hydride site ( $5.7 \text{ kcal mol}^{-1}$ ) still remains.

We have also considered that, after the formation of the dihydrogen-bonded complex at the hydride site, the second HFIP molecule may form a hydrogen bond at the metal site. In other words, the metal and the oxygen atom of the first HFIP molecule may compete as basic centers for the incoming HFIP proton. The optimized geometry of this adduct is represented in Figure 14. This complex lies  $5 \text{ kcal mol}^{-1}$  above the adduct of the HFIP dimer hydrogen bonded at the hydride site (Figure 12, top left). Consequently, it can be

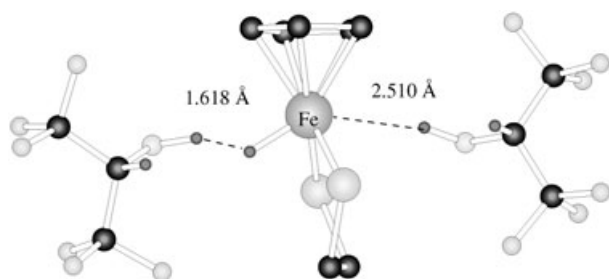


Figure 14. Optimized geometry of a [CpFe(dppe)H]·2(HFIP) isomer with one HFIP molecule hydrogen-bonded at the hydride site and the second one at the metal site. Hydrogen atoms of Cp and  $\text{PH}_2\text{CH}_2\text{CH}_2\text{PH}_2$  are not displayed.

stated that in the presence of an excess of HFIP the initial complex involves the participation of an HFIP dimer forming a dihydrogen bond at the hydride site. As for the TFA case, we find a correlation between the thermodynamics of hydrogen bonding and the kinetics of proton transfer, in favor of the hydride site.

Although the calculations reproduce the main features of the proton transfer process, there is a discrepancy between the calculated and experimental thermodynamics. The experiment shows that the proton transfer from a single TFA molecule is possible, whereas the calculation shows this as endothermic. The experiment also shows exothermicity for proton transfer with two HFIP molecules, whereas the calculation also shows this as slightly endothermic. In both cases, the error has the same origin: the relative stability of the protonation product (the dihydrogen complex) is underestimated with respect to that of the reactant (the monohydride + the proton donor). The cause of this discrepancy is evident from the calibration of the proton affinity discussed above ([Eq. (4)] and Table 5). The model system adopted, with Cp and dppe instead of the actual Cp\* and dppe ligands, presents a lower proton affinity than the real system.

Thus the protonation process in the model system will be less exothermic than in the real one.

## Discussion

**Hydrogen bonding site:** The calculations agree with the experimental study in terms of the identification of the hydride ligand as the preferred hydrogen bonding site. According to the calculations, the interaction with the metal is much less exothermic than the interaction with the hydride. Steric effects probably play the most important role favoring  $\text{M}-\text{H}\cdots\text{H}$  over  $\text{M}\cdots\text{H}$  hydrogen bonds for the [Cp\*FeH(dppe)] system. For this system, hydrogen bonding at the hydride site involves only the hydride ligand, and hydrogen bonding at the metal site only the metal center, since the two sites are mutually *trans*. The proton donor substituents get much closer to the metal coordination sphere when binding occurs at the metal site. Indeed, our computational work shows that the interaction energy at the metal site decreases considerably when moving from dhpe to dppe, whereas a much smaller effect is observed for the interaction energy at the hydride site. For all other previously investigated hydride complexes, hydrogen bonding to the metal site occurs in a *cis* position relative to the hydride site. The cutoff between metal site and hydride site is not so clear in those cases because even for  $\text{M}\cdots\text{H}$  separations of about  $2.6 \text{ \AA}$  (the usual distance for this kind of interaction) there will also be relatively short  $\text{H}\cdots\text{H}$  separation. These hydrogen bonds could be more appropriately described as bifurcated,<sup>[59,63]</sup> and the steric effects may play more similar roles for the two types of interactions.

There does not appear to be a clear correlation between the hydrogen bonding site preference and the basicity factor, which reflects the electronic effects. The basicity factors of hydride ligands reported to date vary from 0.7 to 1.6.<sup>[13]</sup> Relative to the complex [Cp\*FeH(dppe)] ( $E_j = 1.36 \pm 0.02$ ),<sup>[25]</sup> which prefers to use the hydride site, hydrogen bonding has been shown to occur at the metal site for compounds with both higher basicity factors, for example,  $[(\text{NP}_3)\text{ReH}_3]$  ( $E_j = 1.46 \pm 0.01$ ) ( $\text{NP}_3 = \text{N}(\text{CH}_2\text{CH}_2\text{PPh}_2)_3$ )<sup>[10]</sup> and  $(\text{PP}_3)\text{RhH}$  ( $E_j = 1.40$ ),<sup>[64]</sup> and lower ones, for example,  $[\text{WH}_4(\text{dppe})_2]$  ( $E_j = 1.20$ ).<sup>[65]</sup> Thus, the reasons for the preference of the metal or hydride site for hydrogen bonding are not clear at the moment. This topic definitely needs further work, both at the experimental and at the theoretical levels, greater understanding and predictive power may be attained.

The experimentally determined hydrogen bonding energies ( $-6.5 \pm 0.4 \text{ kcal mol}^{-1}$  for HFIP, (cf.  $-5.9 \pm 0.4 \text{ kcal mol}^{-1}$  for TFE and  $-4.6 \pm 0.4 \text{ kcal mol}^{-1}$  for MFE)<sup>[25]</sup>) follow the acidity strength and are of the same order than those reported for other  $\text{M}-\text{H}\cdots\text{H}$  interactions.<sup>[56–58,66,67]</sup> The computed hydrogen bond formation enthalpy values are slightly more negative than those obtained experimentally, possibly because the frequency calculations were carried out in the gas phase where the interaction be-

tween the proton donor and the  $[\text{Cp}^*\text{Fe}(\text{dhpe})\text{H}]$  complex is stronger than in the dichloromethane solvent. The basicity of the complex  $[\text{Cp}^*\text{FeH}(\text{dppe})]$  is sufficiently high to allow proton transfer even in the presence of a proton donor as weak as TFE. The dihydrogen bond formed as the first stage of the protonation reaction determines the direction of the proton transfer process yielding the nonclassical dihydrogen complex.

**Proton transfer activation barrier and equilibrium:** The dihydrogen complex formation is reversible below 260 K, the equilibrium shifts to the right with a temperature decrease or with an acid strength increase. For the  $[\text{Cp}^*\text{FeH}(\text{dppe})]/\text{HFIP}$  system the negative enthalpy ( $\Delta H_1 = -3.2$  to  $-5.5 \text{ kcal mol}^{-1}$ ) and entropy ( $\Delta S_1 = -4.8$  to  $-13.0 \text{ cal mol}^{-1} \text{ K}^{-1}$ ) values for proton transfer step were estimated from the low temperature NMR and UV/Vis studies. The enthalpic profile for the reaction is summarized in Figure 15.

Our previous kinetic investigation of  $[\text{Cp}^*\text{FeH}(\text{dppe})]/\text{HFIP}$ , though limited to a single temperature (298 K), al-

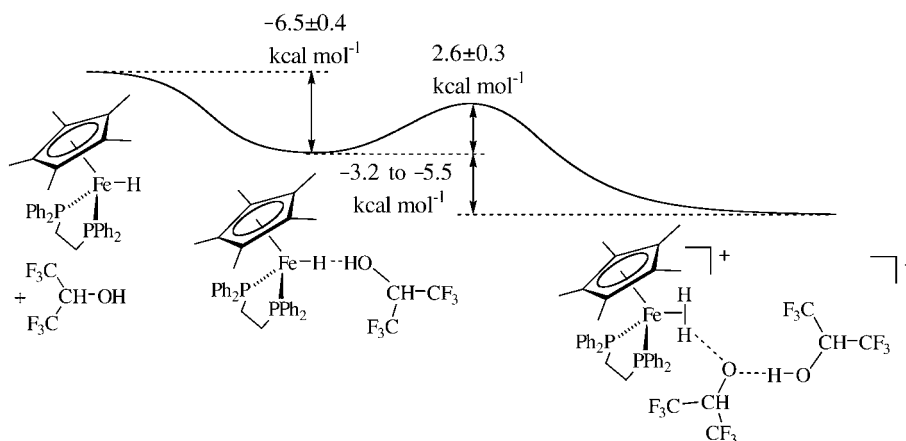


Figure 15. Enthalpic profile for the reaction between  $[\text{Cp}^*\text{Fe}(\text{dppe})\text{H}]$  and HFIP.

lowed us to establish that the proton transfer process is equilibrated and that the forward rate law has a first-order dependence on the alcohol concentration. In combination with the kinetics study involving the proton donors TFE (weaker), PFTB and TFA (stronger), the study also revealed that the proton transfer rate constant increases with the proton donor strength.<sup>[25]</sup> The variable-temperature investigation reported here has provided the activation parameters for the proton transfer process,  $\Delta H_1^\ddagger = 2.6 \pm 0.3 \text{ kcal mol}^{-1}$  and  $\Delta S_1^\ddagger = -44.5 \pm 1.1 \text{ cal mol}^{-1} \text{ K}^{-1}$ . Even though the activation enthalpy is relatively small, the entropic term is such that the activation free energy is in the 12–16  $\text{kcal mol}^{-1}$  range between 200 and 300 K, in agreement with the observation that the NMR resonances of the two equilibrating species are observed separately (slow exchange limit). The proton transfer equilibrium, however, is characterized by a smaller negative entropy ( $-4$  to  $-7$  e.u. from the NMR

study;  $-13$  e.u. from the UV/Vis study), indicating that the transition state is much more ordered than both reagents and products. This is so because the two entities that constitute the starting and final systems are rather loose, the reagents having a hydrogen bond of moderate strength ( $\text{H}\cdots\text{H}$  length of  $1.394 \text{ \AA}$  for the  $[\text{Cp}^*(\text{dppe})\text{FeH}]\cdot 2\text{HFIP}$  adduct) and the product featuring a hydrogen-bonded ion pair with a relatively long  $\text{H}_2$ -anion separation ( $\text{H}\cdots\text{O}$  length of  $1.807 \text{ \AA}$ ). On the contrary, in the TS there is a strong interaction between the two tightly bonded units. In fact, the transition state can be regarded as an  $\text{H}_2$  entity ( $\text{H}-\text{H}$  length  $0.915 \text{ \AA}$ ) simultaneously bonded to both the  $[\text{Cp}^*\text{Fe}(\text{dppe})]^+$  and the  $[\text{AHA}]^-$  units ( $\text{Fe}-\text{H}$  and  $\text{H}-\text{O}$   $1.568$  and  $1.40 \text{ \AA}$ , respectively). Therefore, the two units have lost degrees of freedom in the TS leading to a negative activation entropy.

The barrier is particularly sensitive to the strength of the proton donor as shown by the computational study. The hydrogen bonds have been described as incipient proton transfer reactions.<sup>[68]</sup> Thus it can be expected that a correlation exists between the strength of the  $\text{M}-\text{H}\cdots\text{H}$  interaction and the proton-transfer activation barrier. Indeed we have found such correlation in the two proton transfer reactions studied, with TFA and HFIP as proton donors. In the limit, increasing the dihydrogen bond strength should lead to a complete transfer of the proton onto the hydride and result in the formation of a  $\eta^2$ -dihydrogen ligand.

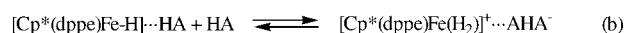
In this respect, it is interesting to analyze the role played by the intervention of a second proton donor molecule, leading to the dihydrogen complex  $[\text{Fe}(\text{H}_2)]^+\cdots[\text{AHA}]^-$ . This intervention is crucial as shown both experimentally and theoretically. During the proton transfer from  $\text{H}-\text{A}\cdots\text{HA}$  to the hydride site, several processes are simultaneously taking place: A) weakening of the  $\text{H}-\text{A}$  bond; B) weakening of the  $\text{Fe}-\text{H}$  bond; C) establishment of the  $\text{Fe}-(\text{H}_2)$  three-center, two-electron bond; D) strengthening of the hydrogen bond between  $\text{A}^-$  (originating from the proton donor) and the second  $\text{HA}$  molecule, leading to the homoconjugated anion  $\text{AHA}^-$ . Only contributions A and D depend on the nature of the proton donor. The calculated parameters (see Results Section) clearly show that the second  $\text{HA}$  molecule increases the strength of the primary dihydrogen bonding interaction (so-called cooperative effect in hydrogen bonding)<sup>[69]</sup> and therefore facilitates proton transfer. It is also possible to imagine that the slightly acidic protons of the dichloromethane solvent molecules interact in the same manner with the proton donor molecule, thereby assisting the proton-transfer process.<sup>[62]</sup> On the other side



of the equilibrium process, the anion stabilization provided by the second proton donor molecule also contributes to lower the activation barrier and to increase the reaction exothermicity (e.g. compare Figure 9 with Figure 11).

**Nature of the conjugate base:** Our previous spectroscopic study (see Introduction) could not provide detailed information on the nature of the proton donor conjugate base,<sup>[25]</sup> that is, whether it is free or hydrogen-bonded (as in **II** or **V**), by itself or associated with the proton donor in a homoconjugated anion. The reason for this lack of information is the fact that the conjugate bases of the fluorinated alcohols used in that study are colorless species and do not exhibit any typical IR absorptions that could signal their hydrogen bonding with the product dihydrogen complex. The *p*-nitrophenol used in the current study show a diagnostic change of the absorption maximum as a function of their protonation status, whereas the anion of TFA exhibits IR absorptions that are also quite sensitive to hydrogen bonding.

The experimental evidence, backed up by the computational work, show that the stronger proton donor TFA is capable of transferring the proton without assistance from a second TFA molecule (equation (a) in Scheme 4). The ion pair [Cp\*(dppe)Fe(H<sub>2</sub>)]<sup>+</sup>...[OCOCF<sub>3</sub>]<sup>-</sup>, in equilibrium with



Scheme 4.

the free ions, forms under conditions of a deficit of TFA. Excess acid then quantitatively produces the free homoconjugated anion, [CF<sub>3</sub>COO(HOCCF<sub>3</sub>)<sub>2</sub>]<sup>-</sup>. On the other hand, the phenol, like the fluorinated alcohols, is a much weaker proton donor than TFA (in DMSO, pK<sub>a</sub> 3.45 for TFA, 10.7 PFTB, 17.9 HFIP and 23.5 TFE).<sup>[51]</sup> It therefore behaves in the same fashion as the fluorinated alcohols for which the intervention of a second proton donor molecule was proven by the kinetic investigation (equation (b) in Scheme 4).

**Solvent effects:** The protonation of a neutral hydride is a reaction involving the generation of charged species from neutral reactants. In this type of process solvent effects are very important. Polar solvents will assist the charge generation process. This behavior can be observed comparing the computed energy profiles for the proton transfer in the gas phase and dichloromethane (see for instance Figure 13). The stabilization caused by the solvent is greater on the product side (ion pair) than at any other point along the pathway. As a result, the monotonically growing energy profile obtained in the gas phase is turned into a double well in DCM. The polarity of the solvent will also play a major role in the charge separation step which leads from the hydrogen-bonded ion pair to the free ions.

## Conclusion

The present study has allowed us to look more closely at the energy profile and mechanism of the proton transfer process to compound [Cp\*Fe(dppe)H]. The general features of this process are identical to those established for the protonation of many other hydride complexes: faster proton transfer to the hydride site, followed by isomerization. The combined experimental and theoretical work has addressed the strength of the hydrogen-bonding interaction, the energetic barrier to the proton transfer step, and the thermodynamics of the proton transfer equilibrium. The preferred site of hydrogen bonding and the strength of the resulting interaction are shown to correlate with the site of the kinetic protonation and with the proton transfer barrier. Finally, important new information on the proton transfer assistance by a second proton donor molecule was revealed by the computational study. The second molecule enhances the ability of the proton donor and stabilizes the transition state and the final product by homoconjugated anion formation. However, sufficiently strong proton donors (in our case, TFA) are capable of transferring the proton without the need of such assistance.

## Acknowledgement

This work was supported by the European Commission's RTN Programme "HYDROCHEM" (HPRN-CT-2002-00176), by INTAS (00-00179), by RFBR (No. 02-03-32194, 03-03-6283), by the Division of Chemistry and Material Science of RAS, by the Spanish DGI (BQU2002-04110-CO2-02), and by a NATO Collaborative Linkage Grant (PST.CLG.978453)

- [1] M. Peruzzini, R. Poli, *Recent Advances in Hydride Chemistry*, Elsevier, Amsterdam, **2001**.
- [2] G. Parkin, J. E. Bercaw, *J. Chem. Soc. Chem. Commun.* **1989**, 255–257.
- [3] M. S. Chinn, D. M. Heinekey, *J. Am. Chem. Soc.* **1990**, *112*, 5166–5175.
- [4] G. Jia, A. J. Lough, R. H. Morris, *Organometallics* **1992**, *11*, 161–171.
- [5] P. Hamon, L. Toupet, J.-R. Hamon, C. Lapinte, *Organometallics* **1992**, *11*, 1429–1431.
- [6] J. R. Hamon, P. Hamon, L. Toupet, K. Costuas, J. Y. Saillard, *C. R. Chimie* **2002**, *5*, 89–98.
- [7] E. T. Papish, F. C. Rix, N. Spetseris, J. R. Norton, R. D. Williams, *J. Am. Chem. Soc.* **2000**, *122*, 12235–12242.
- [8] E. T. Papish, M. P. Magee, J. R. Norton, in *Recent Advances in Hydride Chemistry* (Eds.: M. Peruzzini, R. Poli), Elsevier, Amsterdam, **2001**, pp. 39–74.
- [9] E. S. Shubina, N. V. Belkova, L. M. Epstein, *J. Organomet. Chem.* **1997**, *536–537*, 17–29.
- [10] A. Albinati, V. I. Bakhmutov, N. V. Belkova, C. Bianchini, I. De Los Rios, L. Epstein, E. I. Gutsul, L. Marvelli, M. Peruzzini, R. Rossi, E. S. Shubina, E. V. Vorontsov, F. Zanobini, *Eur. J. Inorg. Chem.* **2002**, 1530–1539.
- [11] R. H. Morris in *Recent Advances in Hydride Chemistry* (Eds.: M. Peruzzini, R. Poli), Elsevier, Amsterdam, **2001**, pp. 1–38.
- [12] L. M. Epstein, N. V. Belkova, E. S. Shubina, in *Recent Advances in Hydride Chemistry* (Eds.: M. Peruzzini, R. Poli), Elsevier, Amsterdam, **2001**, pp. 391–418.



- [13] L. M. Epstein, E. S. Shubina, *Coord. Chem. Rev.* **2002**, *231*, 165–181.
- [14] M. G. Basallote, J. Durán, M. J. Fernández-Trujillo, M. A. Máñez, J. R. De La Torre, *J. Chem. Soc. Dalton Trans.* **1998**, 745–750.
- [15] M. G. Basallote, J. Durán, M. J. Fernández-Trujillo, M. A. Máñez, *J. Chem. Soc. Dalton Trans.* **1998**, 2205–2210.
- [16] M. G. Basallote, J. Durán, M. J. Fernández-Trujillo, M. A. Máñez, *Inorg. Chem.* **1999**, *38*, 5067–5071.
- [17] M. G. Basallote, J. Durán, M. J. Fernández-Trujillo, M. A. Máñez, *J. Organomet. Chem.* **2000**, *609*, 29–35.
- [18] M. G. Basallote, J. Durán, M. J. Fernández-Trujillo, M. A. Máñez, *Organometallics* **2000**, *19*, 695–698.
- [19] M. G. Basallote, M. Besora, J. Durán, M. J. Fernández-Trujillo, A. Lledós, M. A. Mané, F. Maseras, *J. Am. Chem. Soc.* **2004**, *126*, 2320–2321.
- [20] N. Belkova, M. Besora, L. Epstein, A. Lledós, F. Maseras, E. Shubina, *J. Am. Chem. Soc.* **2003**, *125*, 7715–7725.
- [21] N. V. Belkova, E. V. Bakhmutova, E. S. Shubina, C. Bianchini, M. Peruzzini, V. I. Bakhmutov, L. M. Epstein, *Eur. J. Inorg. Chem.* **2000**, 2163–2165.
- [22] V. I. Bakhmutov, E. V. Bakhmutova, N. V. Belkova, C. Bianchini, L. M. Epstein, D. Masi, M. Peruzzini, E. S. Shubina, E. V. Vorontsov, F. Zanobini, *Can. J. Chem.* **2001**, *79*, 479–489.
- [23] E. Gutsul, N. Belkova, M. Sverdllov, L. Epstein, E. Shubina, V. Bakhmutov, T. Gribanova, R. Minyaev, C. Bianchini, M. Peruzzini, F. Zanobini, *Chem. Eur. J.* **2003**, *9*, 2219–2228.
- [24] J. A. Ayllon, C. Gervaux, S. Sabo-Etienne, B. Chaudret, *Organometallics* **1997**, *16*, 2000–2002.
- [25] N. V. Belkova, P. O. Revin, L. M. Epstein, E. V. Vorontsov, V. I. Bakhmutov, E. S. Shubina, E. Collange, R. Poli, *J. Am. Chem. Soc.* **2003**, *125*, 11106–11115.
- [26] A. Lledós, O. Maresca, F. Maseras, R. Poli, E. Collange, unpublished results.
- [27] C. Roger, P. Hamon, L. Toupet, H. Rabaâ, J.-Y. Saillard, J.-R. Hamon, C. Lapinte, *Organometallics* **1991**, *10*, 1045–1054.
- [28] R. A. Binstead, B. Jung, A. D. Zuberbühler, *Specfit/32*, 2000 Spectrum Software Associates, Chapel Hill, NC, **2000**.
- [29] Gaussian 98 (Revision A.9), M. J. Frisch, G. W. Trucks, H. B. Schlegel, G. E. Scuseria, M. A. Robb, J. R. Cheeseman, V. G. Zakrzewski, J. A. Montgomery, R. E. Stratmann, J. C. Burant, S. Dapprich, J. M. Millam, A. D. Daniels, K. N. Kudin, M. C. Strain, O. Farkas, J. Tomasi, V. Barone, M. Cossi, R. Cammi, B. Mennucci, C. Pomelli, C. Adamo, S. Clifford, J. Ochterski, G. A. Petersson, P. Y. Ayala, Q. Cui, K. Morokuma, D. K. Malick, A. D. Rabuck, K. Raghavachari, J. B. Foresman, J. Cioslowski, J. V. Ortiz, A. G. Baboul, B. B. Stefanov, G. Liu, A. Liashenko, P. Piskorz, I. Komaromi, R. Gomperts, R. L. Martin, D. J. Fox, T. Keith, M. A. Al-Laham, C. Y. Peng, A. Nanayakkara, C. Gonzalez, M. Challacombe, P. M. W. Gill, B. Johnson, W. Chen, M. W. Wong, J. L. Andres, M. Head-Gordon, E. S. Replogle, J. A. Pople, Gaussian Inc., Pittsburgh PA, **1998**.
- [30] C. T. Lee, W. T. Yang, R. G. Parr, *Phys. Rev. B* **1988**, *37*, 785–789.
- [31] A. D. Becke, *J. Chem. Phys.* **1993**, *98*, 5648–5652.
- [32] P. Stephens, F. Devlin, C. Chabalowski, M. Frisch, *J. Phys. Chem.* **1994**, *98*, 11623–11627.
- [33] W. R. Wadt, P. J. Hay, *J. Chem. Phys.* **1985**, *82*, 284–298.
- [34] P. J. Hay, W. R. Wadt, *J. Chem. Phys.* **1985**, *82*, 299–310.
- [35] A. Höllwarth, M. Bohme, S. Dapprich, A. Ehlers, A. Gobbi, V. Jonas, K. Kohler, R. Stegmann, A. Veldkamp, G. Frenking, *Chem. Phys. Lett.* **1993**, *208*, 237–240.
- [36] W. Hehre, R. Ditchfie, J. Pople, *J. Chem. Phys.* **1972**, *56*, 2257–2261.
- [37] P. Harihara, J. Pople, *Theor. Chim. Acta* **1973**, *28*, 213–222.
- [38] J. Tomasi, M. Persico, *Chem. Rev.* **1994**, *94*, 2027–2094.
- [39] C. Amovilli, V. Barone, R. Cammi, E. Cancès, M. Cossi, B. Menucci, C. S. Pomelli, J. Tomasi, *Adv. Quantum Chem.* **1998**, *32*, 227–261.
- [40] S. F. Boys, F. Bernardi, *Mol. Phys.* **1970**, *19*, 553–566.
- [41] F. Maseras, K. Morokuma, *J. Comput. Chem.* **1995**, *16*, 1170–1179.
- [42] N. L. Allinger, *mm3(92)*, Quantum Chemistry Program Exchange, Bloomington, IN, **1992**.
- [43] N. Allinger, Y. Yuh, J. Lii, *J. Am. Chem. Soc.* **1989**, *111*, 8551–8566.
- [44] H. Baba, A. Matsuyama, H. Kokubun, *Spectrochim. Acta, Part A* **1969**, *A 25*, 1709–1744.
- [45] I. Majerz, W. Sawka-Dobrowolska, L. Sobczyk, *J. Mol. Struct.* **1997**, *416*, 113–120.
- [46] Z. Dega-Szafran, E. Sokolowska, *J. Mol. Struct.* **2001**, *565*, 17–23.
- [47] E. Gutsul, N. Belkova, G. Babakhina, L. Epstein, E. Shubina, C. Bianchini, M. Peruzzini, F. Zanobini, *Russ. Chem. Bull.* **2003**, *52*, 1204–1206.
- [48] Compare with  $\Delta\lambda_{1/2}$  of PNP = 52 nm at 200 K.
- [49] The absorption of excess [Cp\*FeH(dppe)] contributes to the smaller slope after the breakpoint.
- [50] A. V. Iogansen, *Spectrochim. Acta* **1999**, *55*, 1585–1612.
- [51] F. Bordwell, *Acc. Chem. Res.* **1988**, *21*, 456–463.
- [52] T. Onescu, A.-M. Oancea, L. De Maeyer, *J. Phys. Chem.* **1983**, *87*, 2593–2599.
- [53] J. Z. Dega-Szafran, M. Grundwald-Wyspianska, M. Szafran, *Spectrochim. Acta A* **1991**, *47*, 543–550.
- [54] The averages of all five results are  $\Delta H_1^\ddagger = 4.3 \pm 0.8$  kcal mol<sup>-1</sup> and  $\Delta S_1^\ddagger = -39 \pm 3$  cal mol<sup>-1</sup> K<sup>-1</sup> (see Supporting Information).
- [55] A. V. Iogansen, *Theor. Exp. Chem.* **1971**, *7*, 312–317.
- [56] I. Alkorta, I. Rozas, J. Elguero, *Chem. Soc. Rev.* **1998**, *27*, 163–170.
- [57] F. Maseras, A. Lledós, E. Clot, O. Eisenstein, *Chem. Rev.* **2000**, *100*, 601–636.
- [58] E. Clot, O. Eisenstein, D. H. Lee, R. H. Crabtree in *Recent Advances in Hydride Chemistry* (Eds.: M. Peruzzini, R. Poli), Elsevier, Amsterdam, **2001**, pp. 75–88.
- [59] E. Bakhmutova, V. Bakhmutov, N. Belkova, M. Besora, L. Epstein, A. Lledós, G. Nikonov, E. Shubina, J. Tomas, E. Vorontsov, *Chem. Eur. J.* **2004**, *10*, 661–671.
- [60] E. Bustelo, J. Carbo, A. Lledós, K. Mereiter, M. Puerta, P. Valerga, *J. Am. Chem. Soc.* **2003**, *125*, 3311–3321.
- [61] O. Maresca, F. Maseras, A. Lledós, *New J. Chem.* **2004**, *28*, 625–630.
- [62] T. N. Gribanova, N. V. Belkova, E. I. Gutsul, E. S. Shubina, L. M. Epstein, C. Bianchini, M. Peruzzini, F. Zanobini, R. M. Minyaev, *Eur. J. Inorg. Chem.* unpublished results.
- [63] J. Andrieu, N. V. Belkova, M. Besora, E. Collange, L. M. Epstein, A. Lledós, R. Poli, P. O. Revin, E. S. Shubina, E. V. Vorontsov, *Russ. Chem. Bull.* **2003**, *52*, 2679–2682.
- [64] N. V. Belkova, E. I. Gutsul, E. V. Vorontsov, V. I. Bakhmutov, L. M. Epstein, E. S. Shubina, M. Peruzzini, C. Bianchini, F. Zanobini, A. Lledós, F. Maseras, O. Maresca, unpublished results.
- [65] E. S. Shubina, A. N. Krylov, N. V. Belkova, L. M. Epstein, A. P. Borisov, V. D. Mahaev, *J. Organomet. Chem.* **1995**, *493*, 275–277.
- [66] S. J. Grabowski, *J. Phys. Chem. A* **2000**, *104*, 5551–5557.
- [67] I. Alkorta, J. Elguero, O. Mo, M. Yanez, J. E. Del Bene, *J. Phys. Chem. A* **2002**, *106*, 9325–9330.
- [68] T. Steiner, *Angew. Chem.* **2002**, *114*, 50–80; *Angew. Chem. Int. Ed.* **2002**, *41*, 48–76.
- [69] A. Karpfen, *Adv. Chem. Phys.* **2002**, *123*, 469–510.

Received: July 9, 2004

Published online: December 6, 2004